AFRL-OSR-VA-TR-2015-0006

Phase and Frequency Control of Laser Arrays for Pulse Synthesis

Juliet Gopinath
REGENTS OF THE UNIVERSITY OF COLORADO THE

01/02/2015
Final Report

Air Force Research Laboratory
AF Office Of Scientific Research (AFOSR)/ RTB
Arlington, Virginia 22203
Air Force Materiel Command

REPORT DOCUMENTATION PAGE

Form Approved
OMB No. 0704-0188

PLEASE DO NOT RETURN YOUR FORM TO THE ABOVE ORGANIZATION.

1. REPORT DATE *(DD-MM-YYYY)*	2. REPORT TYPE	3. DATES COVERED *(From - To)*
12/31/14	Final	4/1/11 - 09/30/14

4. TITLE AND SUBTITLE
Phase and Frequency Control of Laser Arrays for Pulse Synthesis
875 North Randolph Street
Arlington VA 22203-1768

5a. CONTRACT NUMBER
FA9550-11-1-0026

5b. GRANT NUMBER
FA9550-11-1-0026

5c. PROGRAM ELEMENT NUMBER
n/a

6. AUTHOR(S)
Gopinath, J. T.

5d. PROJECT NUMBER
n/a

5e. TASK NUMBER
n/a

5f. WORK UNIT NUMBER
n/a

7. PERFORMING ORGANIZATION NAME(S) AND ADDRESS(ES)
University of Colorado Boulder
Department of Electrical, Computer and Energy Engineering
Engineering Center, ECEE 1B55; 425 UCB
Boulder CO 80309

8. PERFORMING ORGANIZATION REPORT NUMBER
n/a

9. SPONSORING/MONITORING AGENCY NAME(S) AND ADDRESS(ES)
AFOSR
875 N Randolph Street, Ste 325 Rm 3112
ARLINGTON VA 22203

10. SPONSOR/MONITOR'S ACRONYM(S)
AFOSR

11. SPONSOR/MONITOR'S REPORT NUMBER(S)
n/a

12. DISTRIBUTION/AVAILABILITY STATEMENT
DISTRIBUTION A

13. SUPPLEMENTARY NOTES

14. ABSTRACT

A phase locked source, consisting of three beams at fo, fo - 80 MHz, and fo + 80 MHz, was demonstrated. Fast feedback was implemented by an FPGA using a single phase-sensitive detector that recorded the peak power of the waveform. We use feedback from a piezo and current-control of a tapered amplifier. We have demonstrated a pulse train of 4.9 ns pulses at 80 MHz, an order of magnitude reduction in phase noise, and the potential for long-term stability. Additionally, we have explored methods for improving the beam quality of a broad area laser array in a wavelength beam combining cavity. Brightness can be increased by imaging the diffraction-limited fast axis back onto the slow axis, with proper astigmatism compensation. The work has been submitted to the 2014 Conference on Lasers and Electro-Optics (CLEO), presented at the 2013 CLEO, one journal paper published in Optics Express, and another is currently under review for publication in Optics Letters.

15. SUBJECT TERMS
Pulse synthesis, coherent combining, spectral combining, pulsed lasers, fast optical feedback, diode lasers

16. SECURITY CLASSIFICATION OF:			17. LIMITATION OF ABSTRACT	18. NUMBER OF PAGES	19a. NAME OF RESPONSIBLE PERSON
a. REPORT	b. ABSTRACT	c. THIS PAGE			Juliet Gopinath
U	U	U	SAR		19b. TELEPHONE NUMBER *(Include area code)* 303 492 5568

Reset

Standard Form 298 (Rev. 8/98)
Prescribed by ANSI Std. Z39.18
Adobe Professional 7.0

INSTRUCTIONS FOR COMPLETING SF 298

1. REPORT DATE. Full publication date, including day, month, if available. Must cite at least the year and be Year 2000 compliant, e.g. 30-06-1998; xx-06-1998; xx-xx-1998.

2. REPORT TYPE. State the type of report, such as final, technical, interim, memorandum, master's thesis, progress, quarterly, research, special, group study, etc.

3. DATES COVERED. Indicate the time during which the work was performed and the report was written, e.g., Jun 1997 - Jun 1998; 1-10 Jun 1996; May - Nov 1998; Nov 1998.

4. TITLE. Enter title and subtitle with volume number and part number, if applicable. On classified documents, enter the title classification in parentheses.

5a. CONTRACT NUMBER. Enter all contract numbers as they appear in the report, e.g. F33615-86-C-5169.

5b. GRANT NUMBER. Enter all grant numbers as they appear in the report, e.g. AFOSR-82-1234.

5c. PROGRAM ELEMENT NUMBER. Enter all program element numbers as they appear in the report, e.g. 61101A.

5d. PROJECT NUMBER. Enter all project numbers as they appear in the report, e.g. 1F665702D1257; ILIR.

5e. TASK NUMBER. Enter all task numbers as they appear in the report, e.g. 05; RF0330201; T4112.

5f. WORK UNIT NUMBER. Enter all work unit numbers as they appear in the report, e.g. 001; AFAPL30480105.

6. AUTHOR(S). Enter name(s) of person(s) responsible for writing the report, performing the research, or credited with the content of the report. The form of entry is the last name, first name, middle initial, and additional qualifiers separated by commas, e.g. Smith, Richard, J, Jr.

7. PERFORMING ORGANIZATION NAME(S) AND ADDRESS(ES). Self-explanatory.

8. PERFORMING ORGANIZATION REPORT NUMBER. Enter all unique alphanumeric report numbers assigned by the performing organization, e.g. BRL-1234; AFWL-TR-85-4017-Vol-21-PT-2.

9. SPONSORING/MONITORING AGENCY NAME(S) AND ADDRESS(ES). Enter the name and address of the organization(s) financially responsible for and monitoring the work.

10. SPONSOR/MONITOR'S ACRONYM(S). Enter, if available, e.g. BRL, ARDEC, NADC.

11. SPONSOR/MONITOR'S REPORT NUMBER(S). Enter report number as assigned by the sponsoring/ monitoring agency, if available, e.g. BRL-TR-829; -215.

12. DISTRIBUTION/AVAILABILITY STATEMENT. Use agency-mandated availability statements to indicate the public availability or distribution limitations of the report. If additional limitations/ restrictions or special markings are indicated, follow agency authorization procedures, e.g. RD/FRD, PROPIN, ITAR, etc. Include copyright information.

13. SUPPLEMENTARY NOTES. Enter information not included elsewhere such as: prepared in cooperation with; translation of; report supersedes; old edition number, etc.

14. ABSTRACT. A brief (approximately 200 words) factual summary of the most significant information.

15. SUBJECT TERMS. Key words or phrases identifying major concepts in the report.

16. SECURITY CLASSIFICATION. Enter security classification in accordance with security classification regulations, e.g. U, C, S, etc. If this form contains classified information, stamp classification level on the top and bottom of this page.

17. LIMITATION OF ABSTRACT. This block must be completed to assign a distribution limitation to the abstract. Enter UU (Unclassified Unlimited) or SAR (Same as Report). An entry in this block is necessary if the abstract is to be limited.

To: technicalreports@afosr.af.mil

Cc: john.luginsland@us.af.mil

Subject: Final Report to Dr. J. Luginsland

Contract/Grant Title: Phase and Frequency Control of Laser Arrays for Pulse Synthesis

Contract/Grant Number: FA9550-11-1-0026

Reporting Period: 1 April 2011 to 30 September 2014

Personnel: Jonathan Pfeiffer (graduate student), Molly Krogstad (graduate student), Kenneth Underwood (graduate student), Andrew Jones (Postdoctoral Associate)

Abstract:

A phase locked source, consisting of three beams at f_o, f_o - *80 MHz*, and f_o + *80 MHz*, was demonstrated. Fast feedback was implemented by an FPGA using a single phase-sensitive detector that recorded the peak power of the waveform. We used feedback from a piezo and current-control of a tapered amplifier. We have demonstrated a pulse train of 4.9 ns pulses at 80 MHz, an order of magnitude reduction in total noise standard deviation with our control loop on, and the potential for long-term stability. Additionally, we have explored methods for improving the beam quality of a broad area laser array in a wavelength beam combining cavity. Brightness can be increased by imaging the diffraction-limited fast axis back onto the slow axis, with proper astigmatism compensation. The work described has been submitted to the 2015 Conference on Lasers and Electro-Optics (CLEO) [1], presented at the 2013 CLEO [2], published in Optics Express [3], and another journal paper is currently under review for publication in Optics Letters [4]. We have also filed a provisional patent on the mode-imaging concept.

Executive Summary:

The goal of the project was to investigate pulse synthesis from cw diode laser arrays with beam combining, as an alternative to modelocking for high powers and pulse energies from diode laser sources. Diode lasers are compact and efficient, with electrical-to-optical efficiencies as high as 85% demonstrated [5]. However, the application space for pulsed diode lasers has been limited by power and pulse energy constraints as well as the inability to achieve short (fs) pulses from the sources in a reliable manner. Fourier pulse synthesis, in which frequency components of the pulses are generated by individual laser elements and added up in phase, has been demonstrated by a few groups [6-9]. Our concept of frequency and phase control from diode laser arrays represents an attractive alternative, using fast feedback from an FPGA and a single phase sensitive metric for optimization, enabling scalability to a large number of elements. Under the program, we have performed two successful experiments investigating this concept, and have plans for a third experiment that is currently in progress.

Phase-Locked Source To study the phase locking of a laser array, we seeded our experiment (shown in Figure 1) with a single frequency diode laser placed in a Littrow cavity (1 MHz linewidth) at 780 nm. The master laser is amplified by a tapered amplifier (TA), before being

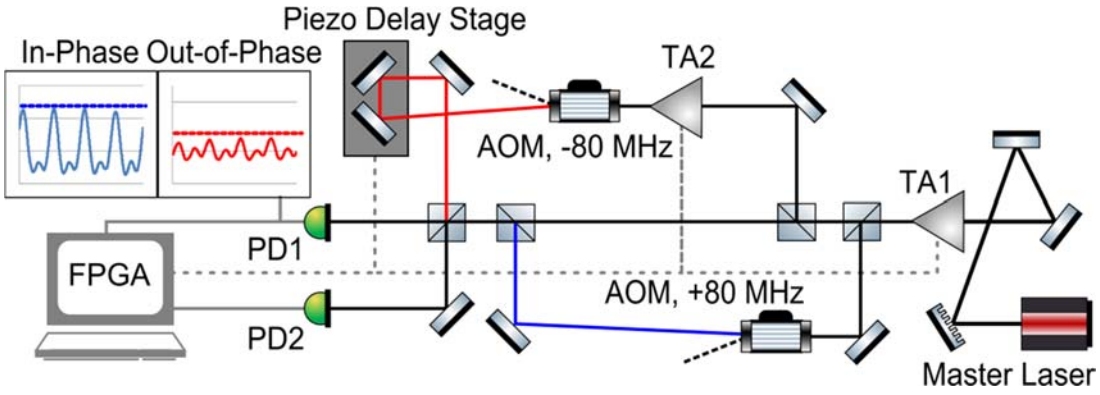

Figure 1. TA, tapered amplifier; AOM, acousto-optic modulator; FPGA, field programmable gate array; PD, photodiode. Experimental set-up of phase locked source. The master laser (bottom right) is single frequency at 780 nm and is amplified by a TA, before being split into three beams. Two of the beams are shifted by +80 MHz and – 80 MHz respectively. TA2 provides fast phase control, while slow phase control is accomplished by a piezo delay stage. Photodiodes 1 and 2 provide peak and average power values to FPGA which controls TA2 and the piezo to provide phase stabilization.

split into three beams. Two of the beams are shifted by +80 MHz and – 80 MHz respectively. TA2 provides fast phase control, while slow phase control is accomplished by a piezo delay stage. Photodiodes 1 and 2 provide peak and average power values to FPGA which controls TA2 and the piezo to provide phase stabilization. Three feedback loops are implemented for the experiment: 12 kHz (TA2, current adjustment to control phase), 80 Hz (piezo), and 40 kHz (TA1, stabilize power in experiment). The feedback to the piezo and the second tapered amplifier is based on stochastic gradient descent, in which a performance metric is monitored (peak power) as random changes are applied to all the inputs. The stochastic gradient is used to update the parameters as follows:

$$u_j^{n+1} = u_j^n + \gamma_j \frac{\delta J}{\delta u_j^n}$$

where u_j is the controller output, j is the element number, n is the iteration number, δu is a small random perturbation in the controller output, δJ is the resultant small change in the cost function (such as autocorrelation or peak power from phase-sensitive detector in our case), and γ_j is a weighting parameter. The key advantage of this algorithm is that it is fast and scalable, using pseudo-gradients rather than actual gradients. It has been demonstrated with hundreds of elements for coherent combining [10]. Results of the phase control experiment are shown in Figure 2. A temporal waveform and RF spectrum are shown for the in-phase and out-of-phase cases. The RF spectrum shows 20 dB of discrimination between the two states, and analysis yields 8% energy fluctuations between pulses, explained by the 5 kHz linewidth of the acousto-optic modulator driver.

To further analyze performance, phase noise spectral density measurements of the individual arms were performed. Light from the arm in question was detected with a fast photodetector and mixed with the AOM driver (80 MHz) to yield both in-phase and quadrature components, as shown in Figure 3 [11]. The in-phase and quadrature components are recorded on a scope, and a periodogram is applied to estimate the PNSD.

$$\frac{\left|FFT\left[\tan^{-1}\left(I/Q\right)\right]\right|^2}{f_{sample}}$$

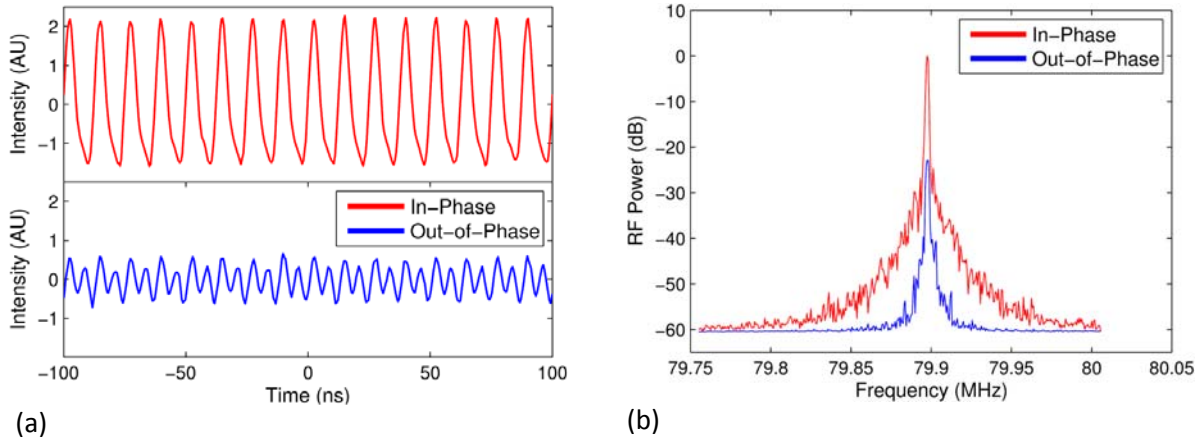

Figure 2. (a) Temporal waveform from the system for both the in-phase and out-of-phase cases. (b) RF spectrum from the system for the in and out of phase cases as well. A 20 dB difference between the in and out-phase cases can be seen from the RF spectrum.

where I is the in-phase component, Q is the quadrature component, FFT is the fast Fourier transform, and f_{sample} is the sampling frequency. Results are shown in Figure 3. The majority of the noise occurs at low frequencies (< 40 Hz) and (< 6 kHz). Low frequency noise is the result of thermal and mechanical effects on the mirrors as well as the frequency fluctuations from the 1 MHz linewidth master laser. Higher frequency noise (100 – 1000 Hz) originates in the tapered amplifier. The most important point is that the frequency of the two feedback loops for the piezo (80 Hz) and phase controlled tapered amplifier (12 kHz) are in areas that encompass the majority of the noise and can therefore effectively correct for the noise in their bandwidth region.

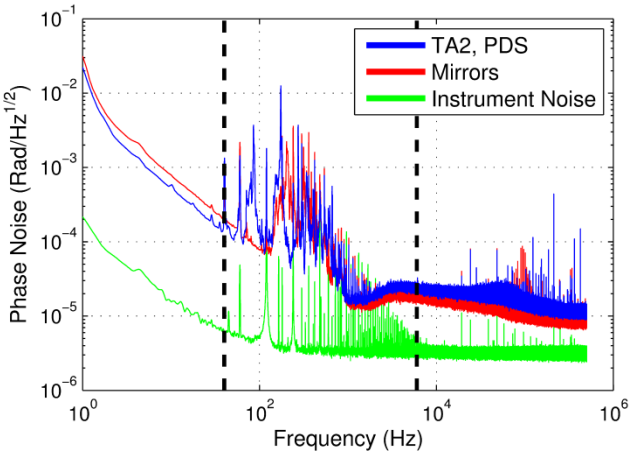

Figure 3. TA2; Tapered amplifier in phase control arm, PDS; Piezo delay stage. Phase noise spectral density of Fourier synthesis system, with phase noise of control arm (TA2, PDS) compared to phase noise of mirror arm and instrument noise floor. Vertical dashed lines show bandwidth of slow (80 Hz) piezo controller and fast (12 kHz) TA controller (both can compensate for 40 Hz and 6 kHz noise respectively.

The effectiveness of control of the normalized cost function is illustrated in Figure 4 for both short (4.7 s) and long (5 min) timescales, as measured by the rectified photodetector and monitored by the FPGA at 40 kHz. Slow variations in the phase are due to thermal effects (<10 Hz), with mid-frequency phase excursions (~200 Hz) arising from mechanical vibrations of optical components in the beam path such as mirrors and lenses. Still higher frequency phase excursions

(>10 kHz) are the result of minor instabilities in the single frequency nature of the master laser. When these phase fluctuations of different components are not being controlled, the system is considered to be in open loop and the cost function fluctuates randomly. Alternatively, when phase fluctuations of different components are being controlled and the system is in a closed loop state, the normalized cost function stays close to one and the pulses are clear and steady. The standard deviation of the phase in the open loop state is 0.82 rad, while the standard deviation of the phase in closed loop is reduced by over an order of magnitude to 0.066 rad.

In conclusion, we have experimentally demonstrated an optical pulse train generator based on the Fourier synthesis of AOM-separated light obtained from an amplified narrow-linewidth cw semiconductor seed laser. We controlled the amplitude and phase of one frequency component using a stochastic gradient descent algorithm implemented on a dedicated FPGA board, and successfully generated a pulse train with an 80 MHz repetition rate and 4.9 ns pulse width. Transitioning with a stochastic parallel gradient descent (SPGD) algorithm to an array of

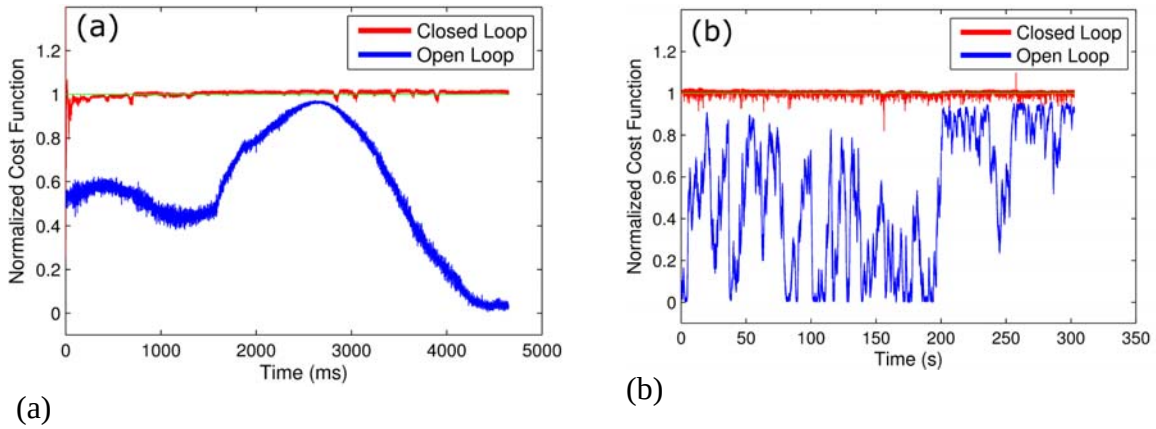

Figure 4. FPGA, field programmable gate array. FPGA phase control system performance (a) over 4.7 seconds and (b) over 5 minutes. When the system is in a closed loop state with FPGA control on, the normalized cost function stays close to one and shows minimal phase deviation. In contrast, large phase fluctuations are seen when the system is in open loop, i.e. FPGA control off.

independent cw lasers would allow for straightforward scaling of the full system, with phase noise limited by the bandwidth of the FPGA feedback. Due to the inherently scalable nature of the SPGD algorithm, the phase detection scheme will not change with many more elements. Our experiment shows that linear Fourier synthesis by FPGA active phase control provides a solution for pulse generation with standard cw diode lasers, and can be directly extended to systems with many more laser devices while retaining a single

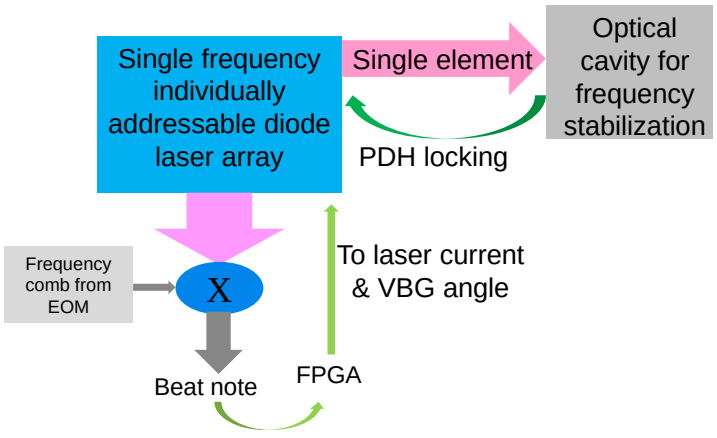

Figure 5. Schematic of proposed experiment for phase and frequency control of an individually addressable laser array.

phase sensitive cost function. The experimental results are under review for publication in Optics Letters and have been submitted to the 2015 Conference on Lasers and Electro-Optics.

Future Pulse Synthesis To generate pulses from laser arrays, the following experiment is proposed (see Figure 5). An anti-reflection diode laser array is placed in a cavity with a chirped volume Bragg grating and etalon, ensuring single frequency, multi-wavelength operation (different elements have different wavelengths). To prevent drift, one element from the diode array is stabilized in frequency by an optical cavity. The frequency spacing of the array is compared with the evenly spaced frequency comb generated by an EOM, electro-optical modulator, in a cavity stabilized to the drive frequency of the EOM. This architecture should allow for scalable pulse generation from laser arrays. While the AFOSR Young Investigator Program has concluded (4/1/11 – 9/30/14), we plan to do a few more experiments on the side with the laser array to understand the phase noise of elements on a common heat sink, and the relationship between linewidth and feedback speed needed for locking. The generation of short pulses from diode lasers at reasonable powers and pulse energies to enable nonlinear optical technologies with good electrical-to-optical efficiencies is an important problem that merits further research. Additionally, lasers where pulse generation is extremely difficult such as quantum cascade lasers, could greatly benefit from the techniques described here. Finally, the maximum speed of phase modulation possible with the thermal and electronic response of diode lasers should be investigated. Current systems are limited to the frequency where the electronic and thermal responses cross-over (somewhere between 100 kHz – few MHz). With the FPGA, we may be able to engineer the response function of the feedback loop as a function of bandwidth to circumvent this issue. The problem described here is one that has captured the attention of the community with solutions ranging from separate phase modulation sections, to specially designed lasers that push the electronic/thermal cross-over out as far as possible in frequency.

Mode Imaging for Brightness Enhancement of Broad-Area Laser Arrays Single mode individually addressable laser arrays for pulse synthesis are difficult to purchase commercially, with only one vendor. However, broad area laser arrays are significantly cheaper and many choices for arrays are available. Improving the beam quality from broad area laser arrays enables them to be used for applications that require higher brightness (power per area-solid angle).

A new method for improving the mode quality from a broad area laser (BAL) array has been studied. The diffraction-limited fast-axis mode of a broad area laser is imaged onto the slow-axis facet, resulting in a twofold reduction of the slow-axis (combined) M^2 value and a corresponding twofold increase in brightness compared with a standard Littman-Metcalf wavelength beam combined cavity. The method is versatile and broadly applicable to BAL single emitters and arrays employing either coherent or wavelength beam combining. The brightness compared with a standard Littman-Metcalf cavity, and a cavity containing a slit is shown in Figure 6. Further enhancements can be obtained by optimizing the output coupling and cavity length. The work has been submitted to the 2013 Conference on Lasers and Electro-Optics [2] and published in Optics Express (2013) [3].

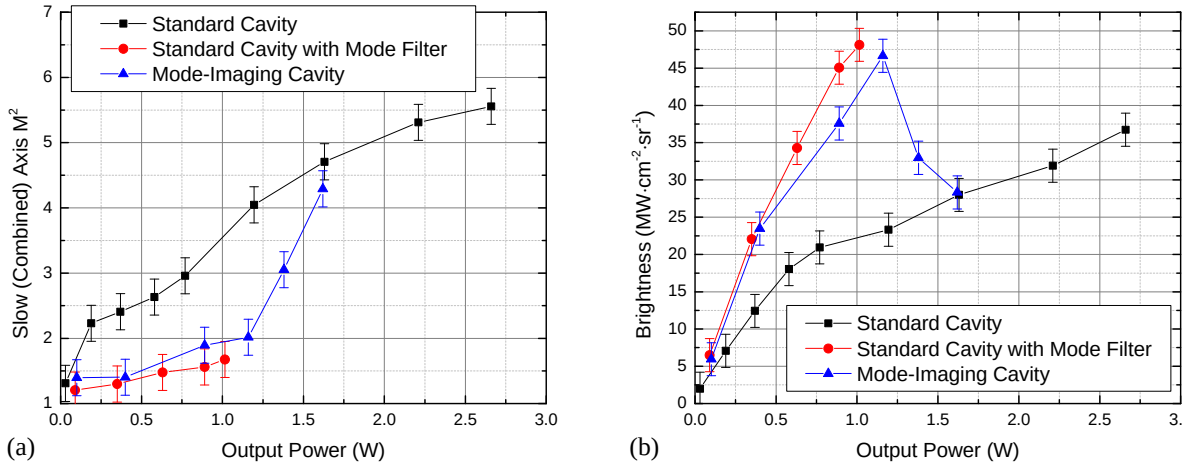

Figure 6. (a) Average slow-axis beam quality as a function of output power for the standard wavelength beam combined (WBC) cavity without (black squares) and with (red circles) intracavity mode filtering and for the mode-imaging cavity (blue upward pointing triangles). Slow-axis M^2 values for both the standard cavity employing mode filtering and the mode-imaging cavities are improved over the standard cavity without mode filtering, and follow very similar trends with the notable exception that the standard cavity with mode filtering could not generate output powers beyond ~ 1 W. (b) Average brightness as a function of output power for all three cavity configurations. The standard WBC cavity employing mode filtering (red circles) and the mode-imaging cavity (blue upward pointing triangles) show maximum brightnesses of greater than 45 $MW \cdot cm^{-2} \cdot sr^{-1}$. Error bars indicate ± one standard deviation from multiple measurements as determined from the cavity configuration with the highest measured standard deviation.

Archival publications (published) during project:

1. A. M. Jones and J. T. Gopinath, "Fast-to-slow axis mode imaging for brightness enhancement of a broad-area laser diode array," *Optics Express* **21**, 17912-17919 (2013).
2. K. J. Underwood, A. M. Jones, and J. T. Gopinath, "Optical pulse generation by Fourier synthesis of three cw semiconductor lasers using an FPGA-based gradient descent phase-locking algorithm," *Submitted to Optics Letters*, December 2014.

Changes in research objectives, if any: None

Change in AFOSR program manager, if any: Yes, Dr. John Luginsland

Extensions granted or milestones slipped, if any: No cost extension from 31 March 2014 to 30 September 2014

Include any new discoveries, inventions, or patent disclosures during project:
US provisional patent application number 62/010,996, titled " Beam Quality Improvement of Broad-Area Laser Diodes by Fast-to-Slow Axis Mode Imaging ", filed 6/11/14, invented by Andrew M Jones and Juliet T Gopinath

References

1. K. J. Underwood, A. M. Jones and J. T. Gopinath, "Synthesis of coherent optical pulses using a field-programmable gate array (FPGA)-based gradient descent phase locking algorithm with three semiconductor lasers," *Submitted to CLEO 2015*, December 2015.
2. A. M. Jones and **J. T. Gopinath**, "Beam quality improvement of broad-area laser diodes by fast-to-slow axis mode imaging," *Presented at Conference on Lasers and Electro-Optics (CLEO) (June 2013)*, JW1J.3.
3. A. M. Jones and **J. T. Gopinath**, "Fast-to-slow axis mode imaging for brightness enhancement of a broad-area laser diode array," *Optics Express* **21**, 17912-17919 (2013).
4. K. J. Underwood, A. M. Jones, and J. T. Gopinath, "Optical pulse generation by Fourier synthesis of three cw semiconductor lasers using an FPGA-based gradient descent phase-locking algorithm," *Submitted to Optics Letters*, December 2014.
5. P. A. Crump, M. Grimshaw, J. Wang, W. Dong, S. Zhang, S. Das, J. Farmer, M. DeVito, L. S. Meng, and J. K. Brasseur, "85% power conversion efficiency 975-nm broad area diode lasers at - 50°C, 76 % at 10°C," in Conference on Lasers and Electro-Optics/Quantum Electronics and Laser Science Conference and Photonic Applications Systems Technologies, Technical Digest (CD) (Optical Society of America, 2006), paper JWB24.
6. C. Hayes and L. Laughman, "Generation of coherent optical pulses,"*Applied Optics* **16**, 263-264 (1977).
7. T. Mukai, R. Wynands, and T. Hänsch, "Optical pulse synthesis with three cw semiconductor lasers using nonlinear phase-locking," *Optics Communications* **95** (1–3), 71-76 (1993).
8. M. Hyodo, N. Onodera, and K. Abedin, "Fourier synthesis of 1.8-THz optical-pulse trains by phase locking of three independent semiconductor lasers," *Optics Letters* **24**, 303-305 (1999).
9. F. Futami and K. Kikuchi, "Generation of 113-GHz, 1.8-ps optical pulse trains by Fourier synthesis of four-wave mixing signals obtained from semiconductor optical amplifiers," *Optics Letters* **22**, 1873-1875 (1997).
10. S. M. Redmond, K. J. Creedon, J. E. Kansky, S. J. Augst, L. J. Missaggia, M. K. Connors, R. K. Huang, B. Chann, T. Y. Fan, G. W. Turner, A. Sanchez-Rubio, "Active coherent beam combining of diode lasers," *Optics Letters*, **36**, 999-1001 (2011).
11. S. J. Augst, J. K. Ranka, T. Y. Fan, and A. Sanchez, "Beam combining of ytterbium fiber amplifiers," *J. Opt. Soc. Am. B* **24**, 1707 (2007).

Beam Quality Improvement of Broad-Area Laser Diodes by Fast-to-Slow Axis Mode Imaging

Andrew M. Jones and Juliet T. Gopinath
University of Colorado - Boulder, Department of Electrical, Computer and Energy Engineering, Boulder, CO, 80309, USA
andrew.mi.jones@colorado.edu

Abstract: A novel technique for beam quality improvement of a broad-area diode array has been demonstrated. For each emitter, the fast-axis mode is imaged back onto the slow axis, improving beam quality while preserving slope efficiency.
OCIS codes: (140.2010) Diode laser arrays; (140.3298) Laser beam combining; (140.5960) Semiconductor lasers.

1. Introduction

Broad-area laser (BAL) diodes offer a simple, compact, efficient means of producing high continuous-wave powers across a broad spectrum spanning the visible to mid-infrared. These powerful, monolithic laser sources have found utility in applications including cutting and welding and as high-power pump sources for other laser systems. However, due to their inherently large lateral dimensions, BALs support multiple transverse modes which reduce beam quality and preclude their use in applications requiring mode-locking or diffraction limited spatial resolution. Improvements in the beam quality of BALs have been demonstrated previously using external cavities which employ intracavity spatial filters [1] or the Talbot effect [2]. Unfortunately, spatial filtering significantly decreases the slope efficiency with respect to the unfiltered cavity, and the Talbot cavity can only be extended to BAL arrays in a coherent combination scheme. In contrast, the technique demonstrated here relies only on reimaging the near diffraction-limited fast-axis mode of the BAL back onto the slow-axis facet. The technique is broadly applicable to BAL single emitters as well as arrays employing either coherent or wavelength beam combining (WBC).

2. Experiment and Results

The laser setup is shown in Fig. 1(a) and follows the standard Littman-Metcalf WBC cavity design [3] with the notable exception that the standard output coupler has been replaced with a half-wave plate and hollow metal retroreflector. The fast and slow-axis lensed BAL diode array is from Jenoptik and consists of 19 emitters, each 100 μm wide with a 500-μm pitch spacing. The front facet of the array is anti-reflection coated ($R < 0.5\%$, typically) while the back facet is coated for high reflectivity. A 100-mm focal length cylindrical transform lens is placed one focal length away from both the array and the 1800 lines/mm holographic diffraction grating. The output from each emitter is spatially overlapped in the first-order diffracted beam from the grating with ~ 95% efficiency. The combined beam passes through a 3º uncoated N-BK7 wedge used to pick-off portions of the beam for monitoring. The transmitted beam then passes through a half-wave plate to the hollow metal retroreflector.

The retroreflector is tilted such that it operates exactly as a hollow right-angle prism, with only two sides of the retroreflector used to reflect the incident beam. The center of the incident beam is coincident with the 90° ± 2 arcsec angle between the two sides of the retroreflector, which is rotated 45° relative to the fast and slow axes of the beam. This causes the fast and slow-axis modes to switch places upon reflection, allowing the near single mode beam emanating from the fast-axis facet of the diode to be imaged back upon the much larger slow-axis facet, and vice versa. This results in increased feedback to the fundamental mode supported in the slow axis of the broad-area emitters. The half-wave plate is used to rotate the transverse electric polarization (parallel to the slow axis) amplified by the laser diodes by 45°, making it parallel to the 90° intersection of the two sides of the retroreflector such that the polarization will not change when the fast and slow-axis modes switch during retroreflection.

The output spectrum of the laser taken at the maximum drive current of 10.5 A, corresponding to an output power of 1.92 W, is shown in Fig. 1(b). Each of the 15 spectral peaks corresponds to the emission from a single emitter. The center wavelengths are given directly by the standard grating equation.

Figure 2(a) shows the light-current characteristics of the mode imaging WBC cavity (red circles) along with those measured for a standard WBC cavity with a 30% reflective flat output coupler. Both cavities use the same BAL diode array, transform lens, and diffraction grating. As shown by the plot, the mode imaging cavity produces a slope efficiency of 0.30 W/A, only 25% less than the 0.40 W/A slope efficiency of the standard cavity.

The M^2 of the beam along the slow axis is shown in Fig. 2(b) for both the mode imaging (red circles) and the standard (black squares) WBC cavity. The beam quality for the mode imaging cavity is better than that of the standard cavity at all measured output powers. At output powers below ~ 0.5 W the beam quality is below 2 and

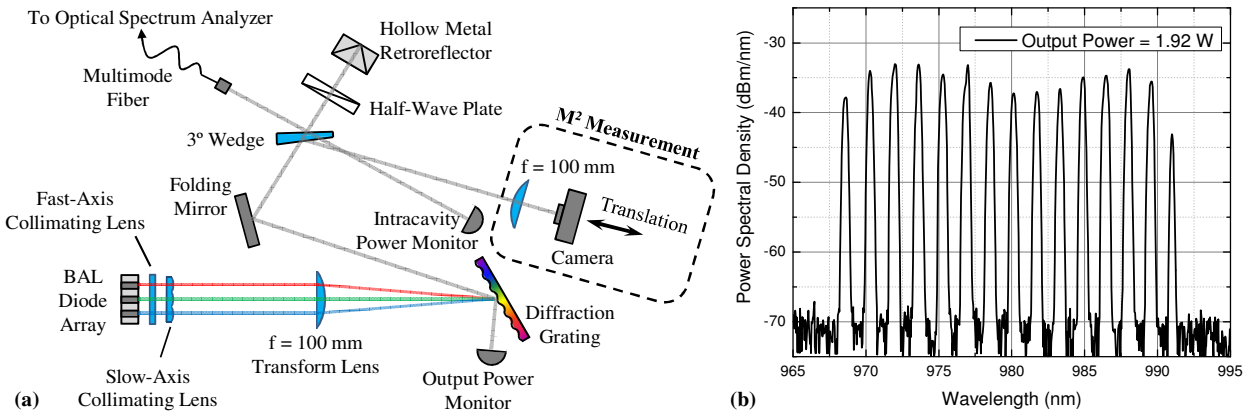

Fig. 1. (a) Fast-to-slow axis mode imaging wavelength beam combined laser cavity. The specular reflection from the grating of the retroreflected beam is used as the laser output. (b) Laser spectrum observed at a drive current of 10.5 A and 1.92 W of output power, taken at 0.1 nm resolution.

relatively flat. At higher drive currents/output powers the beam quality is seen to degrade and approach that of the standard cavity. This is likely due to imperfect overlap of the imaged, fast-axis mode and the fundamental slow-axis mode, permitting enough feedback for higher-order modes to overcome cavity losses at high currents. Compensating observed astigmatism in beam at the retroreflector or shortening the total cavity length to reduce diffraction of the fast-axis beam may further improve the beam quality characteristics of the cavity. In the fast axis, the M^2 was measured to be 1.2 – 1.4 for both cavity configurations at all currents/output powers.

The radiance (or brightness) of the laser is calculated using $B = P/\left(\lambda^2 M_x^2 M_y^2\right)$ [3], where P is the output power, λ is the center wavelength, and M_x^2 and M_y^2 are the slow and fast-axis M^2 values. Figure 2(c) shows the measured radiance for the mode imaging (red circles) and the standard (black squares) WBC cavity. The radiance of the mode imaging cavity is seen to exceed that of the standard cavity at all measured output powers.

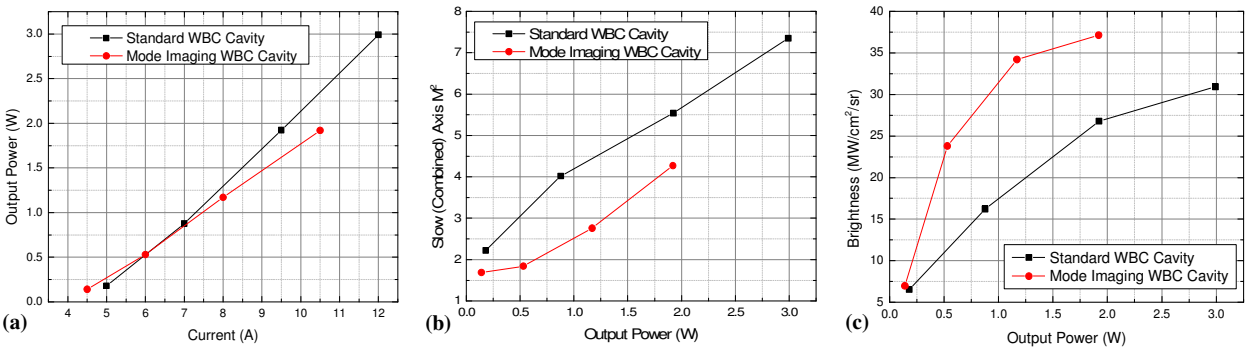

Fig. 2. Measured light-current characteristics (a), slow-axis beam quality (b), and radiance (c) of the standard (black squares) and mode imaging (red circles) wavelength beam combined cavity lasers. All optics are identical between the two lasers with the exception of the 30% reflective flat output coupler used in the standard cavity which is replaced by a half-wave plate and hollow metal retroreflector in the mode imaging cavity.

3. Conclusions

Fast-to-slow axis mode imaging in a WBC cavity configuration has been demonstrated resulting in improved beam quality from individual BAL emitters while preserving the characteristically high slope efficiency of these devices. The improvement is most dramatic at output powers below ~ 0.5 W, where the slow-axis M^2 value is below 2 and relatively flat, as the feedback provided by imaging the fast-axis mode onto the slow-axis facet is enough to suppress lasing in all but the lowest order transverse modes. Compensating astigmatism in the beam at the retroreflector by matching the fast and slow-axis waist sizes or shortening the cavity to reduce beam spreading in the fast-axis should improve mode overlap at the diode facets, potentially further increasing the slope efficiency and allowing the region of relatively little increase in the slow-axis M^2 to persist at higher output powers.

4. References

[1] A. Heuer, A. Sagahti, A. Jechow, D. Skoczowsky, and R. Menzel, "Multi-wavelength, high spatial brightness operation of a phase-locked stripe-array diode laser," *Laser Phys.* **22**, 160 (2012).

[2] J. R. Leger, "Lateral mode control of an AlGaAs laser array in a Talbot cavity," *Appl. Phys. Lett.* **55**, 334 (1989).

[3] T. Y. Fan, "Laser beam combining for high-power, high-radiance sources," *IEEE J. Sel. Top. Quant. Electron.* **11**, 567 (2005).

Fast-to-slow axis mode imaging for brightness enhancement of a broad-area laser diode array

Andrew M. Jones* **and Juliet T. Gopinath**

University of Colorado - Boulder, Department of Electrical, Computer and Energy Engineering, Boulder, CO, 80309, USA

andrew.mi.jones@colorado.edu

Abstract: Broad-area laser (BAL) diodes have found use in numerous applications requiring multi-watt powers, but remain limited by poor spatial beam quality. A novel laser cavity that enhances the brightness of a BAL array has been demonstrated. Wavelength beam combining (WBC) is used to spatially overlap output from the emitters. Improved beam quality is achieved by imaging the fast-axis mode onto the slow axis of the BAL array. The brightness is enhanced twofold over a typical Littman-Metcalf WBC cavity, reaching 47 $MW \cdot cm^{-2} \cdot sr^{-1}$ at an output power of 1.16 W.

OCIS codes: (070.6110) Spatial filtering; (140.2010) Diode laser arrays; (140.3298) Laser beam combining; (140.3410) Laser resonators; (140.5960) Semiconductor lasers.

References and links

1. I. P. G. Photonics, http://www.ipgphotonics.com.
2. N. Lichtenstein, B. E. Schmidt, A. Fily, S. Weiss, S. Arlt, S. Pawlik, B. Sverdlov, J. Muller, and C. S. Harder, "DPSSL and FL pumps based on 980-nm telecom pump laser technology: changing the industry," Proc. SPIE **5336**, 77–83 (2004).
3. J. P. Donnelly, R. K. Huang, J. N. Walpole, L. J. Missaggia, C. T. Harris, J. Plant, R. J. Bailey, D. E. Mull, W. D. Goodhue, and G. W. Turner, "AlGaAs-InGaAs slab-coupled optical waveguide lasers," IEEE J. Quantum Electron. **39**(2), 289–298 (2003).
4. P. Friedmann, J. Schleife, M. Herbstritt, J. Gilly, and M. T. Kelemen, "High efficiency laser sources usable for single mode fiber coupling and frequency doubling," Proc. SPIE **8277**, 82771M, 82771M-10 (2012).
5. H. Taniguchi, H. Ishii, R. Minato, Y. Ohki, T. Namegaya, and A. Kasukawa, "25-W 915-nm lasers with window structure fabricated by impurity-free vacancy disordering (IFVD)," IEEE J. Sel. Top. Quantum Electron. **13**(5), 1176–1179 (2007).
6. P. A. Crump, M. Grimshaw, J. Wang, W. Dong, S. Zhang, S. Das, J. Farmer, M. DeVito, L. S. Meng, and J. K. Brasseur, "85% power conversion efficiency 975-nm broad area diode lasers at - 50°C, 76% at 10°C," in *Conference on Lasers and Electro-Optics/Quantum Electronics and Laser Science Conference and Photonic Applications Systems Technologies*, Technical Digest (CD) (Optical Society of America, 2006), paper JWB24.
7. R. Pandey, D. Merchen, D. Stapleton, S. Patterson, H. Kissel, W. Fassbender, and J. Biesenbach, "Advancements in high-power diode laser stacks for defense applications," Proc. SPIE **8381**, 83810G, 83810G-12 (2012).
8. P. Crump, S. Böldicke, C. M. Schultz, H. Ekhteraei, H. Wenzel, and G. Erbert, "Experimental and theoretical analysis of the dominant lateral waveguiding mechanism in 975 nm high power broad area diode lasers," Semicond. Sci. Technol. **27**(4), 045001 (2012).
9. R. R. Craig, L. W. Casperson, O. M. Stafsudd, J. J. J. Yang, G. A. Evans, and R. A. Davidheiser, "Etched-mirror unstable-resonator semiconductor lasers," Electron. Lett. **21**(2), 62–63 (1985).
10. V. Raab and R. Menzel, "External resonator design for high-power laser diodes that yields 400mW of TEM_{00} power," Opt. Lett. **27**(3), 167–169 (2002).
11. A. Jechow, V. Raab, R. Menzel, M. Cenkier, S. Stry, and J. Sacher, "1 W tunable near diffraction limited light from a broad area laser diode in an external cavity with a line width of 1.7 MHz," Opt. Commun. **277**(1), 161–165 (2007).
12. M. Chi, B. Thestrup, and P. M. Petersen, "Self-injection locking of an extraordinarily wide broad-area diode laser with a 1000-microm-wide emitter," Opt. Lett. **30**(10), 1147–1149 (2005).
13. A. Heuer, A. Sagahti, A. Jechow, D. Skoczowsky, and R. Menzel, "Multi-wavelength, high spatial brightness operation of a phase-locked stripe-array diode laser," Laser Phys. **22**(1), 160–164 (2012).
14. S. Wolff, D. Messerschmidt, and H. Fouckhardt, "Fourier-optical selection of higher order transverse modes in broad area lasers," Opt. Express **5**(3), 32–37 (1999).
15. J. R. Leger, "Lateral mode control of an AlGaAs laser array in a Talbot cavity," Appl. Phys. Lett. **55**(4), 334–336 (1989).
16. B. Liu, Y. Liu, and Y. Braiman, "Coherent beam combining of high power broad-area laser diode array with a closed-V-shape external Talbot cavity," Opt. Express **18**(7), 7361–7368 (2010).

#191385 - $15.00 USD Received 29 May 2013; accepted 1 Jul 2013; published 18 Jul 2013

17. T. Y. Fan, "Laser beam combining for high-power, high-radiance sources," IEEE J. Sel. Top. Quantum Electron. **11**(3), 567–577 (2005).
18. D. Vijayakumar, O. B. Jensen, and B. Thestrup, "980 nm high brightness external cavity broad area diode laser bar," Opt. Express **17**(7), 5684–5690 (2009).
19. M. Fukuda, M. Okayasu, J. Temmyo, and J. Nakano, "Degradation behavior of 0.98-μm strained quantum well InGaAs/AlGaAs lasers under high-power operation," IEEE J. Quantum Electron. **30**(2), 471–476 (1994).
20. V. Daneu, A. Sanchez, T. Y. Fan, H. K. Choi, G. W. Turner, and C. C. Cook, "Spectral beam combining of a broad-stripe diode laser array in an external cavity," Opt. Lett. **25**(6), 405–407 (2000).
21. A. I. Bawamia, B. Eppich, K. Paschke, H. Wenzel, F. Schnieder, G. Erbert, and G. Tränkle, "Experimental determination of the thermal lens parameters in a broad area semiconductor laser amplifier," Appl. Phys. B **97**(1), 95–101 (2009).
22. A. E. Siegman, "How to (maybe) measure laser beam quality," in *DPSS (Diode Pumped Solid State) Lasers: Applications and Issues*, Vol. 17 of OSA Trends in Optics and Photonics (Optical Society of America, 1998), paper MQ1.

1. Introduction

High power laser sources with good spatial beam quality are desirable for many applications including printing and marking, pumping of solid state lasers, imaging and tracking, and for use in nonlinear optical processes including optical parametric amplification and difference frequency generation. Fiber lasers are a top contender for high power applications requiring excellent beam quality, with commercially available fiber lasers producing kilowatt single-mode output powers and wall-plug efficiencies of ~30% [1]. However, fiber lasers require optically pumping with high power semiconductor diode lasers, fundamentally limiting the efficiency and power. Diode lasers themselves are a particularly attractive source platform as they offer a cheap, simple, compact, and efficient means to generate laser output across a broad spectrum, spanning the visible to the mid-infrared, directly from electrical current. While single-mode laser diodes are commercially available, continuous wave output powers remain limited to a few watts [2,3] due to high irradiances resulting from the small transverse dimensions required for single spatial mode operation. Tapered amplifiers can be used in conjunction with single mode laser diodes to increase continuous-wave powers up to several watts [4]. On the other hand, broad-area laser (BAL) diodes can produce continuous-wave powers in excess of 10 W [5], and have found utility in applications including cutting and welding and as high-power pump sources for fiber and solid state laser systems. Electrical-to-optical efficiencies exceeding 76% have been demonstrated at 980 nm [6]. Furthermore, multiple BALs can easily be fabricated on a single chip to create arrays, bars, and stacks that can produce kilowatt-level output powers [7]. However, BALs have inherently large lateral dimensions (100s of microns) and support multiple transverse modes [8]. Multimode emission reduces beam quality and precludes use in applications requiring conventional mode-locking or diffraction-limited spatial resolution.

External cavities provide a means to spatially and spectrally control feedback to diode lasers beyond the intrinsic feedback produced from monolithic structures. Improvements in the beam quality of BALs have been demonstrated using external cavities which employ unstable resonator structures [9], off-axis optical feedback [10–12], intracavity spatial filtering [13,14], and phase locking via the Talbot effect [15,16]. Using these external cavity techniques, the output from individual emitters within a BAL array can be spatially combined to produce a single output beam with increased total spatial radiance or brightness (power per square area per solid angle) [17]. Brightnesses as high as 79 $MW \cdot cm^{-2} \cdot sr^{-1}$ [18] have now been demonstrated at 980 nm from a BAL array in an external cavity. While demonstrated external cavity techniques can improve BAL beam quality, the cavities are relatively complex and have limited usable current ranges or limited potential for beam combing. Talbot cavities can only be implemented through coherent beam combining as they produce phase-locking of adjacent emitters. Off-axis cavities show reduced electrical-to-optical efficiencies due to mismatch of the double-lobed output mode with the truncated output mode used for feedback and the gain profile [10]. Unstable resonators typically require additional nontrivial etching of diode facets [9].

#191385 - $15.00 USD Received 29 May 2013; accepted 1 Jul 2013; published 18 Jul 2013

In this paper, a new technique to improve the beam quality from BALs is demonstrated. The diffraction-limited fast-axis mode of the BAL is imaged onto the slow-axis facet, resulting in a twofold reduction of the slow-axis (combined) M^2 value and a corresponding twofold increase in brightness compared with a standard Littman-Metcalf wavelength beam combined cavity. The method is versatile and broadly applicable to BAL single emitters and arrays employing either coherent or wavelength beam combining.

2. Laser concept

The maximum output power from a single BAL is ultimately limited by either thermal roll-over or catastrophic optical damage. Thermal roll-over results from heating of the diode junction causing increased leakage current. Catastrophic optical damage is caused by nonradiative surface recombination at the diode facet [19]. To avoid these limitations and reach higher optical powers, multiple BALs can be placed side-by-side in a tiling arrangement. While tiling increases the total output power by a factor equal to the number of emitters, the spatial radiance or brightness remains equal to that of a single BAL [17]. The brightness can be increased if each laser's output is spatially overlapped. Beam combining schemes accomplish this by controlling the phase or frequency of the emitters. The result is scaling of the output power and brightness in proportion to the number of emitters [17]. In coherent beam combing, multiple lasers are forced to operate at the same wavelength, and the relative phase of the output emitted by each laser is locked. Wavelength beam combining (WBC) is analogous to wavelength-division-multiplexing in fiber and relies on locking each laser to a different wavelength and spatially combining the outputs into a single beam. Typically, the beams from individual elements are spatially overlapped using a lens and a diffraction grating. The resulting beam has increased spatial radiance at the expense of reduced spectral radiance (power per square area per solid angle per wavelength). To increase the brightness of a WBC source, one can either increase the number of individual laser sources being combined or improve the beam quality produced from each emitter. Using mode imaging in a WBC cavity the beam quality produced from each emitter within a BAL array has been improved, allowing a maximum brightness of more than 45 $MW \cdot cm^{-2} \cdot sr^{-1}$ to be achieved at an output power of > 1 W. Performance was compared to a standard WBC cavity with and without an intracavity slow-axis spatial mode filter. The maximum brightness of the mode-imaging WBC cavity is found to represent nearly a twofold increase in brightness over a similar standard WBC cavity without any mode filtering.

All three WBC cavity configurations use an anti-reflection-coated BAL array containing nineteen 100-μm wide emitters with a center-to-center separation of 500 μm (Jenoptik). The basis of all three cavity configurations is illustrated in Fig. 1(a). First, the fast and slow axes of the array are collimated. In the slow axis, the collimated beam from each emitter is then imaged onto an 1800 lines/mm holographic diffraction grating using a 100-mm focal length transform lens placed one focal length away from both the array and the diffraction grating. Together, the element-to-element spacing of the array, the focal length of the transform lens, and the groove density and diffraction angle of the grating determine the spectral content of the combined output [20]. The first-order diffracted light then passes through a 500-mm focal length secondary fast-axis collimating lens which minimizes the beam divergence in the fast axis. Next, a 1.5:1 slow-axis telescope is used to shrink the slow-axis waist of the beam to more closely match the waist in the fast axis, reducing beam astigmatism. Efficient operation of the mode-imaging cavity requires the described astigmatism correction. An adjustable slit is placed at the focus of the slow-axis telescope. This slit can be left open or closed to a width of 130 μm ± 25 μm and used as an intracavity slow-axis mode filter. Following the slow-axis telescope is an uncoated 3° BK7 wedge used to pick off portions of the combined beam for beam quality and spectral measurements. In the case of the mode-imaging cavity, the dashed box in Fig. 1(a) contains the loop mirror shown in Fig. 1(b). In this configuration, the intracavity slit is left open, and the output power is measured using the zeroth-order diffracted light off of the grating from the returning, spatially-combined beam. In the case of the standard cavities, the dashed box contains only a 30% reflective flat output coupler and a

#191385 - $15.00 USD Received 29 May 2013; accepted 1 Jul 2013; published 18 Jul 2013

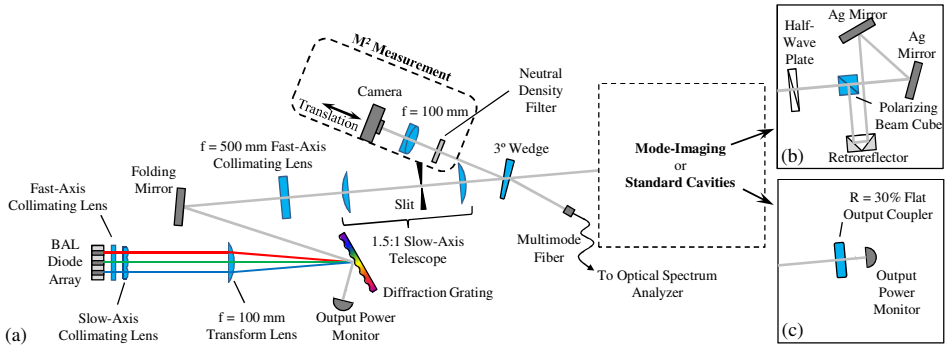

Fig. 1. Standard and mode-imaging wavelength beam combined (WBC) cavities. (a) Basis of both the standard and mode-imaging cavities. The 500-mm focal length secondary fast-axis collimating lens minimizes the fast-axis beam divergence while the 1.5:1 slow-axis telescope reduces the beam waist in the slow axis to approximately 90% of the collimated fast-axis beam waist. (b) Loop mirror used to switch fast- and slow-axis modes. The retroreflector is used as a right-angle prism with the reflection axis rotated 45° relative to the fast and slow axis of the incident beam. (c) Flat output coupler followed by thermal head used to measure output power for the standard WBC cavities.

thermal head used to measure the total output power of the combined beam, as shown in Fig. 1(c). Both the mode-imaging cavity and the standard cavities are relatively long, with effective lengths of 1.7 m and 1.3 m, respectively.

The loop mirror is used to swap the fast- and slow-axis modes emitted from the array and is comprised of a half-wave plate, polarizing beam cube, hollow metal retroreflector, and two silver steering mirrors. The retroreflector is used as a right-angle prism with light reflected by only two sides. The 90° intersection of the two sides represents the reflection axis for the incident beam. The reflection axis is oriented perpendicular to the propagation direction of the incident beam and rotated 45° relative to the fast and slow axis of the BAL emitters. Figure 2 illustrates the mechanism for swapping the fast- and slow-axis spatial modes with the retroreflector. For simplicity, the beam is depicted as astigmatic and centered on the retroreflector's reflection axis. In the actual implementation of the loop mirror, the beam is well off-axis, on the retroreflector. The two silver steering mirrors are then used to overlap this shifted beam with the incident beam on the polarizing beam cube. The result of the loop mirror is that the near single-mode fast-axis beam is rotated 90° and imaged back upon the much larger slow-axis facet, and vice versa. This results in increased feedback to the fundamental mode supported in the slow axis of the broad area emitters and suppression of the higher order modes which have less spatial overlap with the ~1 μm wide fast-axis mode.

For maximum feedback to the laser diodes, the half-wave plate is set to rotate the transverse electric (TE) polarization (parallel to the slow axis) amplified by the laser diodes by 45° as shown in Fig. 2(a). The polarization at the retroreflector is now parallel to the 90° intersection of the two sides of the retroreflector. Now the polarization is invariant when the fast- and slow-axis spatial modes are swapped during retroreflection as indicated in Fig. 2(b). The polarization of the retroreflected beam remains identical to that of the incident beam as it is rotated back to purely TE by the half-wave plate, as shown in Fig. 2(c), allowing all of the retroreflected light to be amplified by the BAL emitters. While the holographic grating used has a diffraction efficiency of ~90% for the TE polarized light emitted by the laser diodes, the diffraction efficiency for the transverse magnetic (TM) polarized light is only ~10%. Therefore, the TM component of the retroreflected light is outcoupled directly from the zeroth-order retroreflected beam off of the grating with ~90% efficiency. By rotating the half-wave plate, the grating can be used as a variable reflectivity output coupler. Since only the TE polarization component of the retroreflected beam is amplified, controlling the amount of retroreflected light that is TE polarized controls the feedback. Some TM light that cannot be amplified is always incident on the array elements. While this was not a problem for the ~1 W

#191385 - $15.00 USD Received 29 May 2013; accepted 1 Jul 2013; published 18 Jul 2013

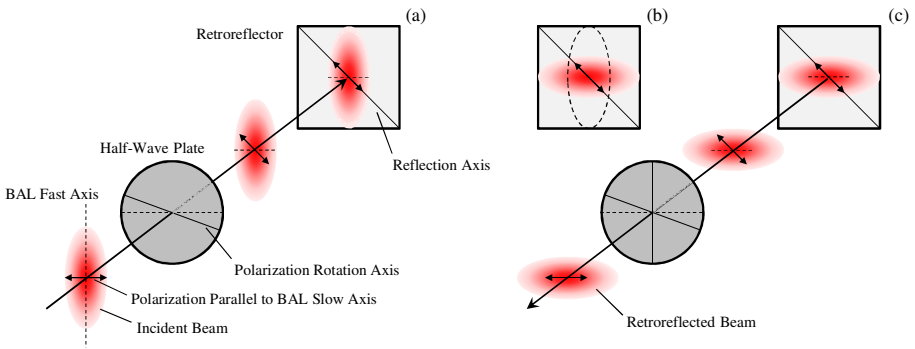

Fig. 2. Diagram illustrating mode swapping with retroreflector. (a) For maximum feedback the half-wave plate rotates the TE polarization of the incident beam to be parallel with the reflection axis of the retroreflector. (b) The beam reflects across the reflection axis of the retroreflector swapping the fast- and slow-axis spatial modes present in the incident beam. Since the polarization is parallel to the reflection axis, it remains unchanged after retroreflection. (c) The retroreflected beam passes back through the half-wave plate where the polarization is rotated back parallel to the TE polarization amplified by the laser diodes. The beam is depicted as astigmatic for clarity, but a stigmatic beam maximizes coupling of the retroreflected beam back into the fast- and slow-axis facets of the BAL emitters.

output powers measured here, at higher powers TM polarized light could cause excess heating in the BAL emitters and degrade the array's performance. This potential problem can be easily mitigated with an optimized grating or an additional polarizing beam splitter placed between the grating and the half-wave plate.

The retroreflector uses an off-axis reflection to provide feedback via the loop mirror. The off-axis implementation is used to prevent beam distortions in the retroreflected beam. When the incident beam is centered on the reflection axis, distortion is evident, as shown in Fig. 3(a). This can be compared with Fig. 3(b), showing an image of the beam reflected off-axis which looks nearly identical to the incident beam, shown in Fig. 3(c) for reference. For an on-axis reflection, interference between the two sides of the incident beam causes the distortion. The two sides of the retroreflector are not at exactly 90° (angular tolerance is specified as ± 2 arcseconds, equal to ± 0.01 mrad), and the two beams walk across each other after reflection.

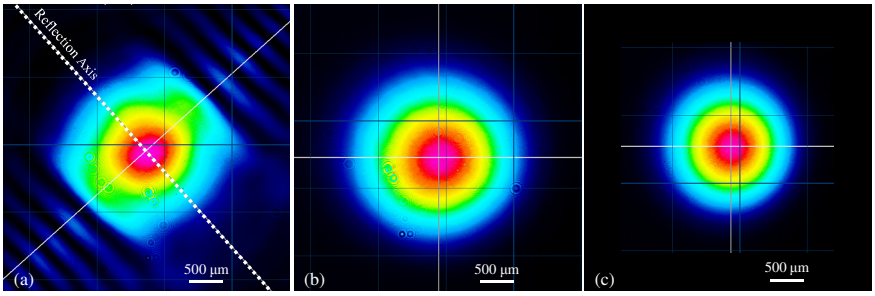

Fig. 3. Characterization of aberrations from the retroreflector. The highest and lowest intensities are shown magenta and black, respectively. Images were taken of a retroreflected HeNe beam with the incident beam centered (a) directly on the retroreflector's reflection axis and (b) far away from the reflection axis. (c) Image of the incident HeNe beam used to test the retroreflector. The beam distortion in (a) is due to interference between the two sides of the reflected beam. The two sides walk across each other due to the imperfect 90° angle between the two reflecting surfaces.

3. Results and discussion

Optical spectra, power, and beam quality were measured for all three WBC cavity configurations. Together, these measured quantities are used to compare the brightness

#191385 - $15.00 USD Received 29 May 2013; accepted 1 Jul 2013; published 18 Jul 2013

achieved for each configuration. In the mode-imaging cavity, the distance between the lenses used in the 1.5:1 slow-axis telescope is re-optimized for output powers greater than 1 W (currents > 8 A). Increasing the separation between the telescope lenses with larger drive currents optimized the output power and beam quality. The optimal separation increased monotonically over the range of currents investigated, reaching a maximum of 8 mm at 11 A and 1.62 W output power. The behavior suggests the formation of a thermal lens within the BAL emitters [21] and increased overlap of higher order modes with the gain profile within the emitters relative to overlap of the fundamental mode.

An output spectrum from the mode-imaging WBC cavity is shown in Fig. 4(a). The spectrum shows multiple individual emission peaks within a bandwidth of about 25 nm. Each emission peak is produced from one emitter in the array. The center wavelength of each peak is determined by the array pitch and cavity optics, and depends on the incident and diffraction angle of the beam from each emitter relative to the grating [20]. The output spectra for all three laser configurations are nearly identical.

The L-I characteristics for all three laser cavity configurations are shown in Fig. 4(b). The threshold current and slope efficiency are 4.1 A and 0.42 W/A, respectively, for the standard Littman-Metcalf WBC cavity without any mode filtering. The threshold currents for both the standard cavity with intracavity mode filtering and the mode-imaging cavity are similar, and the slope efficiencies are nearly identical at 0.26 W/A and 0.24 W/A, respectively. The standard cavity with the intracavity mode filter did not generate output powers beyond 1.02 W even for currents above 8.5 A. This corresponds to the same current where optimization of the slow-axis telescope becomes necessary in the mode-imaging cavity. Thermal lens formation within the BAL emitters may cause reduced transmission through the intracavity slit. Additionally, the anti-reflection coating on the BAL array is imperfect, and drive currents of ~10 A correspond to chip-mode lasing without an external cavity. At 8.5 A, the gain in the fundamental external cavity mode may become equal to the gain of the higher-order chip modes. Further increasing the current would increase the relative gain for the chip modes and thus cause a reduction in the observed power in the fundamental mode circulating within the external cavity.

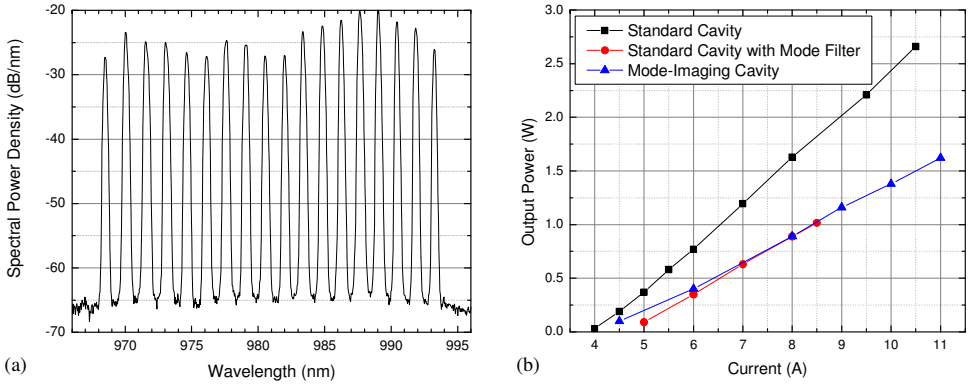

Fig. 4. (a) Spectrum from the mode-imaging cavity taken at a drive current of 9 A producing 1.16 W of output power. The spectrum is typical of all the wavelength beam combined (WBC) laser cavities investigated. Each emission peak corresponds to one emitter in the array with center wavelengths determined by the particular incident and first-order diffraction angle from the grating. The centroid of the spectrum is at 983 nm. (b) L-I curves for the standard WBC cavity without (black squares) and with (red circles) a 130-μm wide intracavity slit used for mode filtering and for the mode-imaging cavity (blue upward pointing triangles).

The beam quality is determined by focusing the beam reflected from the uncoated 3° wedge with a 100-mm focal length achromatic doublet lens and measuring the fast- and slow-axis beam waists with a CMOS camera at several positions. The measured fast- and slow-axis beam caustics were fit using the standard hyperbolic equation [22] with the minimum waist, the axial position corresponding to the minimum waist, and the M^2 factor as free parameters.

#191385 - $15.00 USD Received 29 May 2013; accepted 1 Jul 2013; published 18 Jul 2013

The fast-axis M^2 values range from 1.2 to 1.4 for all cavity configurations, and the measured slow-axis beam quality as a function of output power for all three cavity configurations is shown in Fig. 5(a). The slow-axis M^2 increases with output power for all cavity configurations. Both the standard WBC cavity with mode filter (red circles) and the mode-imaging cavity (blue triangles) show dramatic improvement in beam quality over the standard cavity with no mode filtering. While both cavity configurations show similar trends for the measured slow-axis M^2 values, the standard cavity with slow-axis mode filtering could not generate output powers beyond ~1 W. However, the mode-imaging cavity data shows that the M^2 values remain low until an output power of 1.16 W is reached, after which the beam quality quickly degrades. The drive current corresponding to these transitions coincides closely with the threshold current for lasing observed for the BAL array without any external cavity feedback. Improving the anti-reflection coating on the front facet of the diodes or angle cleaving the laser facets should permit higher powers to be reached before observing substantial degradation in the beam quality.

The radiance or brightness, B, of the WBC lasers is given by [17],

$$B = \frac{P}{\lambda^2 M_x^2 M_y^2}, \tag{1}$$

where P is the output power, λ is the center wavelength, and M_x^2 and M_y^2 are the slow- and fast-axis M^2 values. Brightness computed using Eq. (1) as a function of total output power for all three cavity configurations is shown in Fig. 5(b). Again, the standard cavity with mode filtering and the mode-imaging cavity are seen to have similar brightness for output powers up to ~1 W, reaching peak values in excess of 45 $MW \cdot cm^{-2} \cdot sr^{-1}$, approximately a factor of two more than that of the standard cavity without mode filtering at the same output power. The brightness for the mode-imaging cavity is seen to degrade at output powers beyond 1.16 W as a direct consequence of the rapid increase in the slow-axis M^2 values.

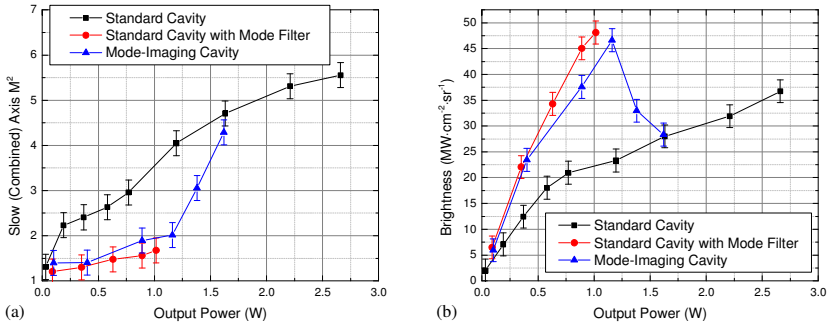

Fig. 5. (a) Average slow-axis beam quality as a function of output power for the standard wavelength beam combined (WBC) cavity without (black squares) and with (red circles) intracavity mode filtering and for the mode-imaging cavity (blue upward pointing triangles). Slow-axis M^2 values for both the standard cavity employing mode filtering and the mode-imaging cavities are improved over the standard cavity without mode filtering, and follow very similar trends with the notable exception that the standard cavity with mode filtering could not generate output powers beyond ~1 W. (b) Average brightness as a function of output power for all three cavity configurations. The standard WBC cavity employing mode filtering (red circles) and the mode-imaging cavity (blue upward pointing triangles) show maximum brightnesses of greater than 45 $MW \cdot cm^{-2} \cdot sr^{-1}$. Error bars indicate ± one standard deviation from multiple measurements as determined from the cavity configuration with the highest measured standard deviation.

4. Conclusion

A novel technique to dramatically improve beam quality produced from BALs in which the emitted fast-axis mode is reimaged back onto the slow-axis dimension of the laser facet has

#191385 - $15.00 USD Received 29 May 2013; accepted 1 Jul 2013; published 18 Jul 2013

been demonstrated. Together, the fast-axis lens and BAL facets function as optical Fourier filters, suppressing lasing of higher-order transverse modes within the external cavity. The technique is simple and broadly applicable to BAL single emitters and arrays employing external cavity feedback, including both coherent and wavelength beam combined systems. Slow-axis M^2 values of ≤ 2 at output powers up to 1.16 W have been achieved from a BAL array in a WBC cavity employing this mode-imaging technique, producing a maximum brightness of 47 $MW \cdot cm^{-2} \cdot sr^{-1}$ at a center wavelength of 983 nm. The beam quality improvement from the mode-imaging cavity configuration closely parallels that observed from a standard WBC cavity employing a slow-axis telescope and slit as an optical Fourier filter due to filtering characteristics of the mode-imaging cavity. To the authors' knowledge, this work represents the first application of intracavity Fourier filtering to an array of single-stripe BAL emitters, with demonstrated output powers and brightnesses in excess of those reported for the near single mode emitters within the multi-stripe array used in [13].

Both intracavity Fourier filtering and the newly demonstrated mode-imaging technique have been demonstrated to improve the beam quality from a BAL array within a WBC setup. The mode-imaging technique achieved ~20% higher output power compared with the mode filter cavity before significant beam quality degradation was observed. Simplifying the mode-imaging cavity setup by employing fewer optical components may further increase the maximum output power and brightness. For example, utilizing matched fast- and slow-axis collimating lenses which produce astigmatic beams directly from the emitters would allow the secondary fast-axis collimating lens and the two slow-axis telescope lenses to be removed from the current setup. Fewer optics and better fast- and slow-axis mode matching would reduce intracavity losses, provide simpler and more robust cavity alignment, and allow much shorter cavity lengths to be realized. At high powers, competition from chip-mode lasing is expected to spoil the beam quality. Increasing the lasing threshold of the BAL array through better anti-reflection coatings or utilizing emitters with angled facets should increase the usable output power and maximum brightness.

Acknowledgments

This work is supported by the Air Force Office of Scientific Research (AFOSR) under grant number FA9550-11-1-0026 through the Young Investigator Program.

#191385 - $15.00 USD Received 29 May 2013; accepted 1 Jul 2013; published 18 Jul 2013

Synthesis of coherent optical pulses using a field-programmable gate array (FPGA)-based gradient descent phase-locking algorithm with three semiconductor lasers

Kenneth J. Underwood,[1,*] Andrew M. Jones,[2] and Juliet T. Gopinath[2]
[1]*University of Colorado Boulder, Department of Physics, Boulder, CO, 80309, USA*
[2]*University of Colorado Boulder, Department of Electrical, Computer and Energy Engineering, Boulder, CO, 80309, USA*
**Corresponding author: kenneth.underwood@colorado.edu*

Abstract: We demonstrate optical pulse synthesis through coherent combination of AOM-separated light by phase-locking feedback from an FPGA. An order of magnitude improvement in phase stability is shown, limited by the noise of the AOM driver.
OCIS codes: (140.3298) Laser beam combining; (140.2020) Diode lasers; (140.3538) Lasers, pulsed

1. Introduction

Semiconductor pulsed laser systems have been investigated for their potential use in many applications such as spectroscopy, free-space communications, LIDAR, and remote sensing. Such systems cannot achieve high peak powers and pulse energies, however, due to the onset of nonlinear effects such as two-photon absorption, gain saturation, carrier-transport effects, and optical damage in the semiconductor. Unique approaches to solving this problem using chips with larger areas, different gain media, and lower confinement factors [1-3] have seen some success, but such methods are ultimately still limited by these same nonlinear effects due to the unavoidable requirement for high intracavity intensity.

An alternative technique for optical pulse generation, Fourier synthesis, effectively sidesteps this limitation by using narrow-linewidth cw light to synthesize the optical pulse waveform outside of the chip. The Fourier synthesis approach has been investigated with CO_2 lasers [4], semiconductor lasers [5, 6], and four-wave mixing using semiconductor optical amplifiers [7]. Most implementations rely on a combination of phase-locked loops and nonlinear optics to force the coherence necessary for pulse generation. The elaborate nature of such systems restricts the scalability of the design, with the complexity and cost rapidly increasing with additional frequencies. Here we successfully demonstrate an alternative approach to phase locking using a single phase-sensitive metric and stochastic gradient descent algorithm implemented on a dedicated field-programmable gate array (FPGA) board. Our approach uses a narrow-linewidth source separated by acousto-optic modulators (AOM) into three cw beams, phase stabilized via current feedback to a tapered amplifier (TA), and recombined to synthesize a stable 80 MHz pulse train. The waveform of the pulse train is maintained for over 5 minutes by fast active feedback from the FPGA controller, limited only by mode-hopping instabilities in the master laser.

2. Experimental Setup

In this experiment shown in Fig. 1(a), light from a narrow-linewidth cw semiconductor master laser is amplified using a tapered amplifier (TA) before being split into three beams, two of which are frequency shifted using 80MHz acousto-optic modulators to form f_0, $f_1 = f_0 - 80$ MHz, and $f_2 = f_0 + 80$ MHz. The phase of frequency f_1 is controlled by a piezo-driven delay stage which directly changes the optical path length and a current-modulated second tapered amplifier which adjusts the phase of the beam by thermal variation of its index of refraction. The three beams are then superimposed on a common optical axis, forming a pulse train with 4.9 ns pulses and 80 MHz repetition rate. The characteristics of the pulse train are monitored using a half-wave rectified fast photodetector which provides a low frequency phase dependent signal which acts as the single phase sensitive metric that supplies a cost function to the FPGA phase control algorithm. Maximization of this cost function locks the phase of the three beams together and thus stabilizes the pulse waveform.

3. Results

Figure 1(c) shows the synthesized waveform during in-phase and out-of-phase operation at a frequency separation of 80 MHz. The phase noise spectral density (PNSD) of the control arm with the second tapered amplifier and piezo delay stage (PDS), the stable arm with only passive optical media (mirrors, beam splitters), and the AOM drive signal itself is shown in Fig. 1(b) and was measured by mixing the AOM driver signal with the 80 MHz photodiode beat signal in an IQ mixer architecture [9]. The vertical dashed lines in the figure demonstrate the motivations for choosing the particular operating bandwidth for the piezo delay stage and tapered amplifier

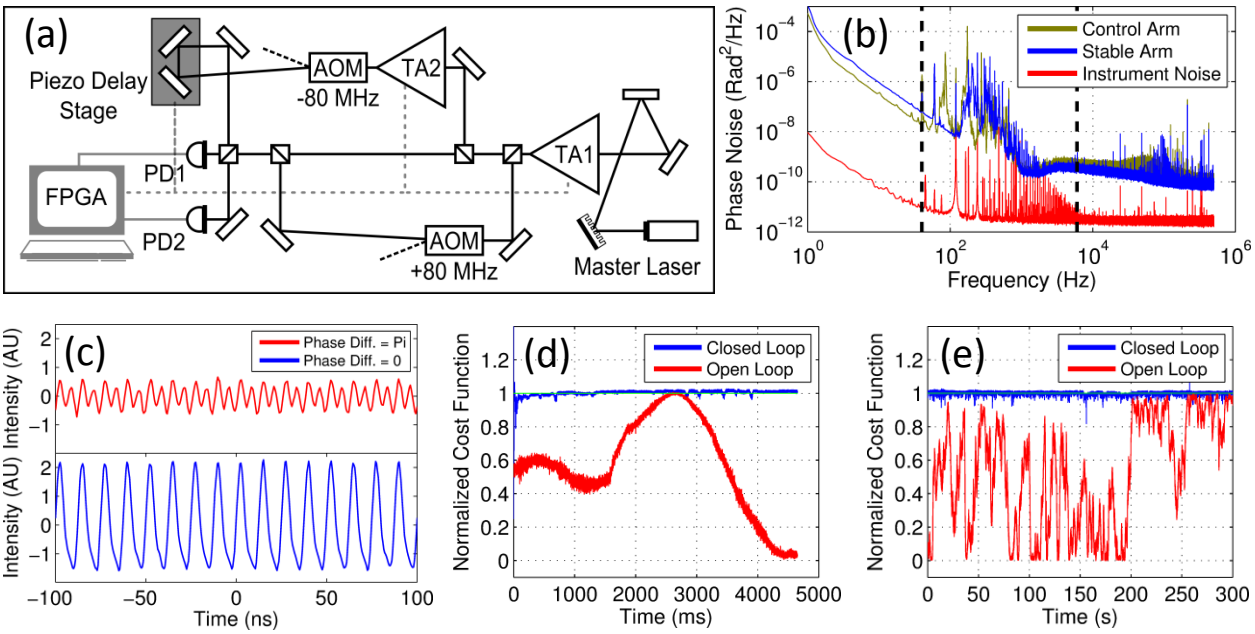

Figure 1(a) Experimental setup for Fourier synthesis system: AOM, acousto-optic modulator; TA1, TA2, tapered amplifiers; PD1, PD2, photodetectors; FPGA, field-programmable gate array. (b) Phase noise spectral density of Fourier synthesis system, with phase noise of control arm compared to phase noise of mirror arm and instrument noise floor. Vertical dashed lines show bandwidth of slow (40 Hz) piezo controller and fast (6 kHz) TA controller. (c) Synthesized waveforms from Fourier combined beams. FPGA phase control system performance over (d) 4.7 seconds and (e) 5 minutes. When the system is in a closed loop state with FPGA control on, the normalized cost function stays close to one and shows minimal phase deviation. In contrast, large phase fluctuations are seen when the system is in open loop, i.e. FPGA control off.

controllers. The 40 Hz PDS encompasses most large slow fluctuations, and the 6 kHz TA controller handles any medium strength, mid-frequency-range phase noise. Higher frequency effects are minimal, but could also be corrected using a faster FPGA. Figure 1(d) and (e) demonstrate the effectiveness of the control system on the normalized cost function (representing the peak power of the synthesized waveform) in open loop and closed loop states over time scales of 4.7 seconds and 5 minutes, respectively. When phase fluctuations are not being controlled, the system is considered to be in open loop and the cost function fluctuates randomly. Alternatively, when phase fluctuations are being controlled and the system is in a closed loop state, the normalized cost function stays close to one. The standard deviation of the phase in the open loop state is 0.82 rad, while the standard deviation of the phase in closed loop is reduced by over an order of magnitude to 0.066 rad.

4. Conclusions

We have experimentally demonstrated an optical pulse train generator based on the Fourier synthesis of AOM-separated light obtained from an amplified narrow-linewidth cw semiconductor seed laser. We controlled the amplitude and phase of one frequency component using a stochastic gradient descent algorithm implemented on a dedicated FPGA board, decreasing the phase deviation by an order of magnitude, and successfully generated a pulse train with an 80 MHz repetition rate and 4.9 ns pulse width. Transitioning with a stochastic parallel gradient descent (SPGD) algorithm to an array of independent cw lasers would allow for straightforward scaling of the full system while retaining a single phase-sensitive metric.

5. References

[1] K. Wilcox, A. Tropper, H. Beere, D. Ritchie, B. Kunert, B. Heinen, and W. Stolz, Opt. Express 21, 1599-1605 (2013).
[2] D. I. Nikitichev, Y. Ding, M. A. Cataluna, E. U. Rafailov, L. Drzewietzki, S. Breuer, W. Elsaesser, M. Rossetti, P. Bardella, T. Xu, I. Montrosset, I. Krestnikov, D. Livshits, M. Ruiz, M. Tran, Y. Robert, and M. Krakowski, Laser Phys. 22, 715-724 (2012).
[3] J. Plant, J. Gopinath, B. Chann, D. Ripin, R. Huang, and P. Juodawlkis, Opt. Lett. 31, 223-225 (2006).
[4] C. Hayes and L. Laughman, Appl. Opt. 16, 263-264 (1977).
[5] T. Mukai, R. Wynands, and T. Hänsch, Opt. Comm. 95, Iss. 1–3, 71-76 (1993).
[6] M. Hyodo, N. Onodera, and K. Abedin, Opt. Lett. 24, 303-305 (1999).
[7] F. Futami and K. Kikuchi, Opt. Lett. 22, 1873-1875 (1997).
[8] D. von der Linde, App. Phys. B, 39, 201-217 (1986).
[9] S. Augst, T. Fan, and A. Sanchez, Opt. Lett. 29, 474-476 (2004).

Submitted to Optics Letters, December 2014.

Optical pulse generation by Fourier synthesis of three cw semiconductor lasers using an FPGA-based gradient descent phase-locking algorithm

Kenneth J. Underwood,[1,*] Andrew M. Jones,[2] and Juliet T. Gopinath[2]

[1]*University of Colorado Boulder, Department of Physics, Boulder, CO, 80309, USA*
[2]*University of Colorado Boulder, Department of Electrical, Computer and Energy Engineering, Boulder, CO, 80309, USA*
**Corresponding author: kenneth.underwood@colorado.edu*

Received Month X, XXXX; revised Month X, XXXX; accepted Month X, XXXX; posted Month X, XXXX (Doc. ID XXXXX); published Month X, XXXX

Optical pulse synthesis is demonstrated through superposition of AOM-separated light from an amplified single-frequency semiconductor master laser. 4.9 ns pulses with an 80 MHz repetition rate are formed by phase-locking feedback from a single phase-sensitive metric applied via fast current modulation of a tapered amplifier using a stochastic gradient descent algorithm realized on a field-programmable gate array (FPGA). The waveforms are maintained by constant active feedback from the FPGA. This technique can be easily extended to many more semiconductor laser emitters in a diode laser array.

OCIS Codes: (140.3298) Laser beam combining, (140.2020) Diode lasers, (140.3538) Lasers, pulsed.
http://dx.doi.org/10.1364/OL.99.099999

Direct diode sources have found application in many aspects of laser physics due to their low cost, high efficiency, and high gain. High power optical pulse train generation from traditional quantum well lasers remains difficult however due to the onset of limiting effects such as two-photon absorption, gain saturation, carrier-transport effects, and optical damage in the semiconductor, keeping typical values for the average power below ~10 mW and peak powers below ~1W [1, 2]. Further difficulties arise in the nonlinear interaction between the optical field, current density, and refractive index, resulting in self-phase modulation that can be difficult to compensate [3, 4]. Systems expressly designed for high-power operation have been developed, such as passively mode-locked vertical-external-cavity surface-emitting lasers (VECSELs) [5, 6], quantum dot lasers with tapered gain sections [7], and passively mode-locked slab-coupled optical waveguide lasers [8], the last of which for example has generated 10 ps pulses with an average power of 250 mW at a repetition rate of 4.29 GHz, reaching 5.8 W peak power. While impressive, these techniques are ultimately still limited by nonlinear effects and possible optical damage from their high intracavity intensities [9]. Fourier synthesis presents an appealing alternative technique for optical pulse generation which removes the inherent power restrictions of similar conventionally mode-locked devices by using narrow-linewidth independent cw lasers to generate the pulse outside of the chip. In the same way that optical pulses are analyzed by being broken down into their constituent sine-wave frequencies (Fourier analysis), these same sine-waves can be combined together in-phase to instead generate the original pulses (Fourier synthesis). Fourier synthesis is particularly attractive for time-resolved measurements and optical communication due to its direct control over both repetition rate and pulse width within the system time-bandwidth product, and has seen application in work towards achieving a functional arbitrary optical waveform generator [10].

Optical pulse generation by Fourier synthesis was first demonstrated by Hayes and Laughman in 1977 with CO_2 waveguide lasers and multiple electronic phase-locked loops [11], but was limited in scale by the necessity for individual detectors for every emitter and limited in bandwidth by the speed of the phase detector. Semiconductor lasers were first used for pulse synthesis by Mukai et al. [12] using a nonlinear phase-locking process, but again lacked scalability, as each additional emitter required an additional nonlinear crystal and optical phase-locked loop (OPLL) system [13]. Experiments by Futami et al. [14] and Hyodo et al. [15] generating phase-locked frequencies through four-wave mixing had similar issues with extending the technique. Arbitrary waveforms have also been generated using phase and amplitude modulators on spatially separated components of coherent few-harmonic combs, but have again seen difficulty in expanding the technique to higher orders [10]. This scalability issue has limited successful pulse generation to five frequencies [11].

Here we report on a direct-diode pulse synthesis system using a single linear phase-sensitive metric, controlled though a stochastic gradient descent (SGD) algorithm implemented on a field-programmable gate array (FPGA) controller. This technique uses a narrow-linewidth source separated by acousto-optic modulators (AOM) into three cw beams and Fourier combined into a stable 160 MHz pulse train. The waveform of the pulse train is maintained over a prolonged period by fast active feedback from an FPGA controller receiving cost function data from the single linear phase-sensitive metric.

The beam combining experimental setup is shown in Figure 1. A single-mode anti-reflection-coated 780nm laser diode in Littrow configuration, the "master laser," is coupled into a 1-W GaAs tapered amplifier (TA). With minimal temperature and mechanical stabilization the master laser has a linewidth of ~1 MHz and cw output power of 25 mW. A 40 dB Faraday optical isolator follows the master laser to prevent unwanted optical feedback

from the tapered amplifier and downstream components causing power and frequency fluctuations in the beam. Tapered amplifiers have been used for more than a decade in master oscillator-power amplifier (MOPA) systems to increase the power of narrow linewidth single mode semiconductor seed lasers [16, 17], and have seen application in frequency comb locking, boosting the power in f-to-2f interferometers with minimal impact on the phase coherence due to their sub-Hz linewidth [18].

In this experiment, amplified light out of the first TA (TA1) is split by a polarizing beam cube, where one arm seeds a second tapered amplifier of the same model and the other proceeds to the frequency shifting phase. Where the first tapered amplifier is used to provide enough power to downstream components to ensure usable signal-to-noise ratio, the second TA provides both optical gain and a controllable current-modulated phase shift through thermal and electronic variation in the refractive index of the tapered amplifier chip [19]. After this amplification/phase-control stage, the single frequency light passes through two acousto-optic modulators (Gooch and Housego model R23080-2-LTD) which shift the light into three beams separated in frequency by 80 MHz, forming f_0, $f_1 = f_0 - 80$ MHz, and $f_2 = f_0 + 80$ MHz. The phase of frequency f_1 is then controlled again by a piezo-driven delay stage before being superimposed on a common optical axis with the other two beams, forming the pulse train. The characteristics of the Fourier synthesized waveform are determined using a series of Si photodetectors.

Due to the amplitude-sensitive phase locking requirements of the FPGA controller algorithm and the high operating frequency of the AOM driver compared to the FPGA clock frequency (50 MHz), two detection signals must be provided to the FPGA; the first provides the peak power and the second the average power. The maximum of the combined output is measured by half-wave rectification of an AC-coupled 1GHz photodiode signal, forming a phase-dependent signal with a bandwidth of 160 kHz. As the phase of the beat signal formed by two of the arms drifts from that of the other two, the generated waveform decreases in peak power and the lower frequency signal from the rectified detector decreases. This low frequency phase-dependent signal can then be read by the FPGA controller, and thus provides the cost function J for the SGD algorithm. The second detector measures the total average power of the combined beam with a 1.9 MHz bandwidth, passing this information to the FPGA controller as well. A third detector with a >1.2 GHz bandwidth provides fast direct waveform measurement monitored on a 1GHz oscilloscope, not shown in the figure. This data is used for diagnostic purposes only.

To stabilize the phase and amplitude of the generated pulses, we use a dedicated FPGA with a threefold control mechanism. We implement the necessary active phase control through an SGD algorithm, shown to provide robust control in many facets of adaptive optics [20, 21]. A slow SGD algorithm applied to a piezo-driven delay stage at 80 Hz corrects for large slow fluctuations (0-40Hz) in the phase between the three beams as measured by our cost function above. A faster smaller amplitude SGD algorithm is applied instead to the drive current of TA2, operating at 12 kHz, to correct for smaller fast fluctuations (40-6000 Hz) in the phase. This correction current alters the index of refraction of the tapered amplifier chip, providing these small phase corrections.

The stochastic gradient descent algorithm [20, 22] in its most general form is

$$u^{(n+1)} = u^{(n)} - \gamma(\delta J/\delta u), \qquad (1)$$

where u is the controller output, n the iteration number, δu the small random perturbation in the control output, δJ the resultant small change in the cost function, and the weighting parameter γ [20]. With random perturbations, the expectation value of the stochastic vector $\delta J/\delta u$ approximates the true gradient of J. Randomness is provided in the FPGA by way of a uniform randomness array procedurally generated by a 32-bit linear feedback shift register. Jump strength is held below a maximum experimentally derived value to avoid ringing in the piezo or damaging the TA. The randomness of the algorithm is expressly designed to avoid effects of local minima as well as correct for other shortcomings of standard gradient descent, including slow convergence time.

As the TA phase correction current adjustments also slightly alter the power emitted by the second TA, very fast corrections to the total power (40 kHz) are made to the first TA to reduce the effect of this power-current relationship. These corrections are made by way of a tuned proportional-integral-derivative (PID) feedback loop controller also realized on the FPGA, where the gain coefficients of the PID loop were arrived at through standard Ziegler-Nichols tuning [23]. The 0.1 MHz AC-coupling in PD1 also acts to decrease the impact of total power fluctuations in the phase-dependent signal, though does not remove them entirely due to the nonlinear relationship of the average input power to the peak intensity signal from the half-wave rectifier.

Synthesized waveforms given in Figure 2 show in-phase and out-of-phase operation at a frequency separation of 80 MHz. The RF spectrum of the fundamental provided in Figure 3 demonstrates the >20dB discrimination between in-phase and out-of-phase peaks during operation, indicating the balanced power between the three arms. These signals are amplified for peak discrimination using a 25 dB gain low-noise RF amplifier (ZFL-1000LN+, 2.9 dB noise figure). Analysis of this amplitude noise spectrum using a Von der Linde approach [24] through the noise burst model gives the width of the noise envelope to be 5 kHz, corresponding to 8% intrinsic energy fluctuations in the pulses. These fluctuations can be explained completely by the 5 kHz linewidth of the RF driving frequency for the acousto-optic modulator.

The phase noise spectral density (PNSD) of the system is shown in Figure 4. By splitting off the AOM driver frequency and mixing it with the 80 MHz photodiode beat signal in an IQ mixer architecture we were able to measure the phase noise from 1 Hz up to 1 MHz in the tapered amplifier-piezo delay stage (TA2, PDS) arm, the frequency separation arm with only passive optical media (mirrors, beam splitters), and the AOM drive signal itself to act as a noise baseline [25]. Data was recorded at 1MS/s

over 20 seconds using a Tektronix MDO 4104B-6 oscilloscope, where the PNSD was approximated with a periodogram smoothed to reduce measurement noise. This PNSD measurement of the individual arms of the Fourier synthesis system is analogous to a phase-noise analysis of an actively mode-locked diode laser. In Figure 4, the phase noise present in the primary control arm (TA2, PDS) is compared with the noise in the arm which interacts with only mirrors as well as the bare drive signal to the AOM as baseline instrument phase noise. The majority of phase noise activity is present at very low frequencies (~0-40 Hz) and medium-range operating frequencies (<6 kHz), where low frequency terms can be seen to be present in both the beam which interacts with TA2 and the PDS and the beam which interacts with only mirrors. Stronger mid-range peaks can be seen in the TA2, PDS spectral density, suggesting that low frequency phase noise is primarily a result of thermal and mechanical effects in the mirrors present in both arms as well as free space eddies, and 100-1000 Hz phase noise originates primarily in the tapered amplifier. The vertical dashed lines in the figure demonstrate the motivations for choosing the particular operating bandwidth for the piezo delay stage and tapered amplifier controllers. The 40 Hz PDS encompasses most large slow fluctuations, and the 6 kHz TA controller handles any medium strength, mid-frequency-range phase noise. Higher frequency effects are minimal, but could also be corrected using a faster FPGA.

Figure 5 demonstrates the effectiveness of the control system on the normalized cost function (representing the peak power of the synthesized waveform) in open loop and closed loop states over different time scales, (5a) over 4.7 seconds and (5b) over 5 minutes, as measured by the rectified photodetector and monitored by the FPGA at 40 kHz. Slow variations in the phase are due to thermal effects (<10 Hz), with mid-frequency phase excursions (~200 Hz) arising from mechanical vibrations of optical components in the beam path such as mirrors and lenses. Still higher frequency phase excursions (>10 kHz) are the result of minor instabilities in the single frequency nature of the master laser. When these phase fluctuations of different components are not being controlled, the system is considered to be in open loop and the cost function fluctuates randomly. Alternatively, when phase fluctuations of different components are being controlled and the system is in a closed loop state, the normalized cost function stays close to one and the pulses are clear and steady. The standard deviation of the phase in the open loop state is 0.82 rad, while the standard deviation of the phase in closed loop is reduced by over an order of magnitude to 0.066 rad.

In conclusion, we have experimentally demonstrated an optical pulse train generator based on the Fourier synthesis of AOM-separated light obtained from an amplified narrow-linewidth cw semiconductor seed laser. We controlled the amplitude and phase of one frequency component using a stochastic gradient descent algorithm implemented on a dedicated FPGA board, and successfully generated a pulse train with an 80 MHz repetition rate and 4.9 ns pulse width. Transitioning with a stochastic parallel gradient descent (SPGD) algorithm to an array of independent cw lasers would allow for straightforward scaling of the full system, with phase noise limited by the bandwidth of the FPGA feedback. Due to the inherently scalable nature of the SPGD algorithm, the phase detection scheme would not change with many more elements. Our experiment shows that linear Fourier synthesis by FPGA active phase control provides a solution for pulse generation with standard cw diode lasers, and can be directly extended to systems with many more laser devices while retaining a single phase sensitive cost function.

The authors gratefully acknowledge technical support from David Glugla. This work is sponsored by the US Air Force Office of Scientific Research Young Investigator Program, grant #FA9550-11-1-0026. K. J. Underwood acknowledges support from the NIST/RASEI-sponsored Colorado Measurement Fellowship.

References

1. G. Tandoi, C. N. Ironside, J. H. Marsh, A. C. Bryce, IEEE J. of Quant. Elec. 48(3), 318-327 (2012).
2. A. Schmitt-Sody, A. Velten, Y. Liu, L. Arissian, and J. C. Diels, Res. Lett. in Opt., vol.2008, 865092, (2008).
3. G. Agrawal and N. Olsson, IEEE J. Quantum Electron. 25, 2297-2306 (1989).
4. P. Vasilyev, I. White, and J. Gowar, *Rep. Prog. Phys.* 63, 1997-2042 (2000).
5. K. Wilcox, A. Quarterman, H. Beere, D. Ritchie, and A. Tropper, IEEE Phot. Tech. Lett. 22, 1021-1023 (2010).
6. K. Wilcox, A. Tropper, H. Beere, D. Ritchie, B. Kunert, B. Heinen, and W. Stolz, Opt. Express 21, 1599-1605 (2013).
7. D. I. Nikitichev, Y. Ding, M. A. Cataluna, E. U. Rafailov, L. Drzewietzki, S. Breuer, W. Elsaesser, M. Rossetti, P. Bardella, T. Xu, I. Montrosset, I. Krestnikov, D. Livshits, M. Ruiz, M. Tran, Y. Robert, and M. Krakowski, Laser Phys. 22, 715-724 (2012).
8. J. Plant, J. Gopinath, B. Chann, D. Ripin, R. Huang, and P. Juodawlkis, Opt. Lett. 31, 223-225 (2006).
9. F. Ahmad, Y. Tseng, M. Kats, and F. Rana, Opt. Lett. 33, 1041-1043 (2008).
10. H. Chan, Z. Hsieh, W. Liang, A. Kung, C. Lee, C. Lai, R. Pan, and L. Peng, Science 331 (6021), 1165-1168 (2011).
11. C. Hayes and L. Laughman, Appl. Opt. 16, 263-264 (1977).
12. T. Mukai, R. Wynands, and T. Hänsch, Opt. Comm. 95, Iss. 1–3, 71-76 (1993).
13. N. Satyan, W. Liang, A. Kewitsch, G. Rakuljic, A. Yariv, Sel. Top. in Quant. Elec. 15-2, 240-247 (2009).
14. F. Futami and K. Kikuchi, Opt. Lett. 22, 1873-1875 (1997).
15. M. Hyodo, N. Onodera, and K. Abedin, Opt. Lett. 24, 303-305 (1999).
16. A. Wilson, J. Sharpe, C. McKenzie, P. Manson, and D. Warrington, Appl. Opt. 37, 4871-4875 (1998).
17. J. Kangara, A. Hachtel, M. Gillette, J. Barkeloo, E. Clements, S. Bali, B. Unks, N. Proite, D. Yavuz, P. Martin, J. Thorn, and D. Steck, Am. J. Phys., 82, 805 (2014)
18. F. Cruz, M. Stowe, and J. Ye, Opt. Lett. 31, 1337-1339 (2006).
19. M. Fukuda, T. Mishima, N. Nakayama, and T. Masuda, App. Phys. B 100, 2, 377-382 (2010).
20. M. Vorontsov, G. Carhart, and J. Ricklin, Opt. Lett. 22, 907-909 (1997).
21. R. Su, P. Zhou, X. Wang, Y. Ma, and X. Xu, Opt. Lett. 37, 497-499 (2012).

22. B. Dong, D. Ren, and X. Zhang, Res. Astron. Astrophys., 11, 997-1002 (2011).
23. J. Ziegler and N. Nichols, Trans. ASME, 64, 759-768 (1942).
24. D. von der Linde, App. Phys. B, 39, 201-217 (1986).
25. S. Augst, T. Fan, and A. Sanchez, Opt. Lett. 29, 474-476 (2004).
26. Mention of commercial products is for information only; it does not imply endorsement or recommendation.

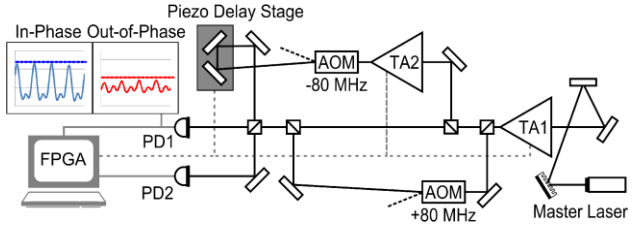

Fig. 1. Experimental setup for Fourier synthesis system: AOM, acousto-optic modulator; TA1, TA2, tapered amplifiers; PD1, PD2, photodetectors; FPGA, field-programmable gate array.

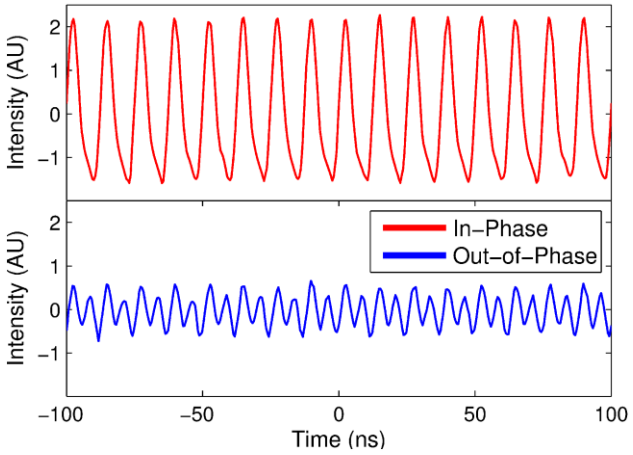

Fig. 2. Synthesized waveforms from Fourier combined beams. In-phase corresponds to $\Delta\varphi=0$, where $\Delta\varphi$ describes the phase difference between the beat note f_0-f_1 and the beat note f_0-f_2. Correspondingly, out-of-phase refers to $\Delta\varphi=\pi$.

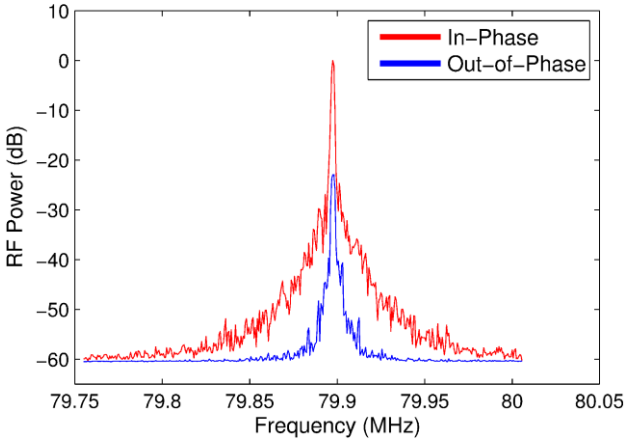

Fig. 3. RF beat note spectrum for $\Delta\varphi=0$ (in-phase) and π (out-of-phase). Note large 20 dB discrimination between in-phase and out-of-phase peaks as well as narrow linewidth noise envelope given by radio-frequency driver for acousto-optic modulators.

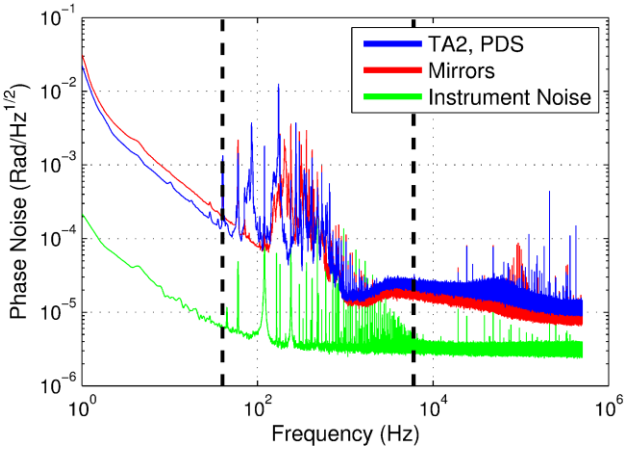

Fig. 4. TA2; Tapered amplifier in phase control arm, PDS; Piezo delay stage. Phase noise spectral density of Fourier synthesis system, with phase noise of control arm (TA2, PDS) compared to phase noise of mirror arm and instrument noise floor. Vertical dashed lines show bandwidth of slow (40 Hz) piezo controller and fast (6 kHz) TA controller.

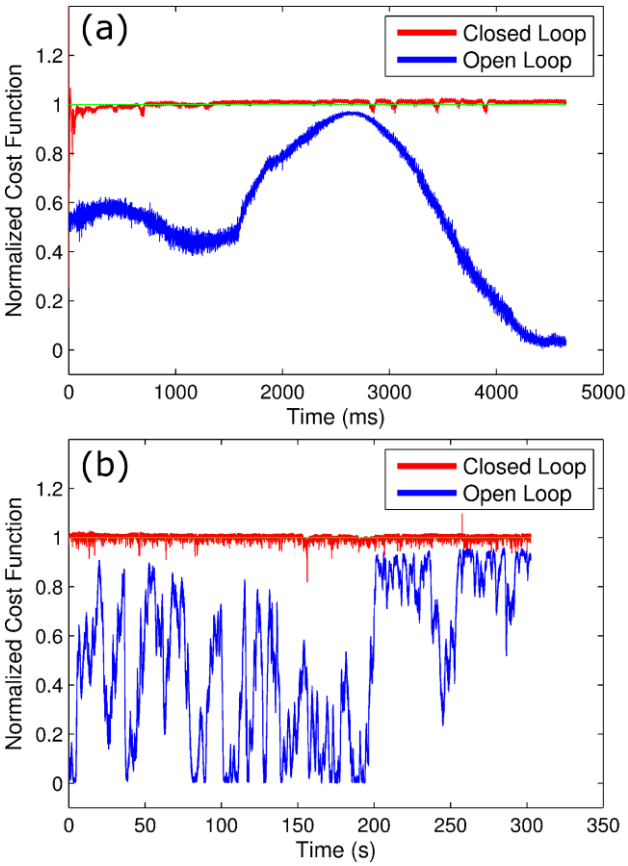

Fig. 5. FPGA phase control system performance (a) over 4.7 seconds and (b) over 5 minutes. When the system is in a closed loop state with FPGA control on, the normalized cost function stays close to one and shows minimal phase deviation. In contrast, large phase fluctuations are seen when the system is in open loop, i.e. FPGA control off.

1. G. Tandoi, C. N. Ironside, J. H. Marsh, A. C. Bryce, "Output Power Limitations and Improvements in Passively Mode Locked GaAs/AlGaAs Quantum Well Lasers," IEEE J. of Quant. Elec. 48(3), 318-327 (2012).
2. A. Schmitt-Sody, A. Velten, Y. Liu, L. Arissian, and J. C. Diels, "High-Power Hybrid Mode-Locked External Cavity Semiconductor Laser Using Tapered Amplifier with Large Tunability," Res. Lett. in Opt., vol.2008, 865092, (2008).
3. G. Agrawal and N. Olsson, "Self-Phase Modulation and Spectral Broadening of Optical Pulses in Semiconductor Laser Amplifiers," IEEE J. Quantum Electron. 25, 2297-2306 (1989).
4. P. Vasilyev, I. White, and J. Gowar, "Fast phenomena in semiconductor lasers," *Rep. Prog. Phys.* 63, 1997-2042 (2000).
5. K. Wilcox, A. Quarterman, H. Beere, D. Ritchie, and A. Tropper, "High Peak Power Femtosecond Pulse Passively Mode-Locked Vertical-External-Cavity Surface-Emitting Laser," IEEE Phot. Tech. Lett. 22, 1021-1023 (2010).
6. K. Wilcox, A. Tropper, H. Beere, D. Ritchie, B. Kunert, B. Heinen, and W. Stolz, "4.35 kW peak power femtosecond pulse mode-locked VECSEL for supercontinuum generation," Opt. Express 21, 1599-1605 (2013).
7. D. I. Nikitichev, Y. Ding, M. A. Cataluna, E. U. Rafailov, L. Drzewietzki, S. Breuer, W. Elsaesser, M. Rossetti, P. Bardella, T. Xu, I. Montrosset, I. Krestnikov, D. Livshits, M. Ruiz, M. Tran, Y. Robert, and M. Krakowski, "High Peak Power and Sub-Picosecond Fourier-Limited Pulse Generation from Passively Mode-Locked Monolithic Two-Section Gain-Guided Tapered InGaAs Quantum-Dot Lasers," Laser Phys. 22, 715-724 (2012).
8. J. Plant, J. Gopinath, B. Chann, D. Ripin, R. Huang, and P. Juodawlkis, "250 mW, 1.5μm monolithic passively mode-locked slab-coupled optical waveguide laser," Opt. Lett. 31, 223-225 (2006).
9. F. Ahmad, Y. Tseng, M. Kats, and F. Rana, "Energy limits imposed by two-photon absorption for pulse amplification in high-power semiconductor optical amplifiers," Opt. Lett. 33, 1041-1043 (2008).
10. H. Chan, Z. Hsieh, W. Liang, A. Kung, C. Lee, C. Lai, R. Pan, and L. Peng, "Synthesis and Measurement of Ultrafast Waveforms from Five Discrete Optical Harmonic," Science 331 (6021), 1165-1168 (2011).
11. C. Hayes and L. Laughman, "Generation of coherent optical pulses," Appl. Opt. 16, 263-264 (1977).
12. T. Mukai, R. Wynands, and T. Hänsch, "Optical pulse synthesis with three cw semiconductor lasers using nonlinear phase-locking," Opt. Comm. 95, Iss. 1–3, 71-76 (1993).
13. N. Satyan, W. Liang, A. Kewitsch, G. Rakuljic, A. Yariv, "Phase locking of semiconductor lasers using homodyne detection and negative electrical feedback," Sel. Top. in Quant. Elec. 15-2, 240-247 (2009).
14. F. Futami and K. Kikuchi, "Generation of 113-GHz, 1.8-ps optical pulse trains by Fourier synthesis of four-wave mixing signals obtained from semiconductor optical amplifiers," Opt. Lett. 22, 1873-1875 (1997).
15. M. Hyodo, N. Onodera, and K. Abedin, "Fourier synthesis of 9.6-GHz optical-pulse trains by phase locking of three continuous-wave semiconductor lasers," Opt. Lett. 24, 303-305 (1999).
16. A. Wilson, J. Sharpe, C. McKenzie, P. Manson, and D. Warrington, "Narrow-linewidth master-oscillator power amplifier based on a semiconductor tapered amplifier," Appl. Opt. 37, 4871-4875 (1998).
17. J. Kangara, A. Hachtel, M. Gillette, J. Barkeloo, E. Clements, S. Bali, B. Unks, N. Proite, D. Yavuz, P. Martin, J. Thorn, and D. Steck, "Design and construction of cost-effective tapered amplifier systems for laser cooling and trapping experiments," Am. J. Phys., 82, 805 (2014)
18. F. Cruz, M. Stowe, and J. Ye, "Tapered semiconductor amplifiers for optical frequency combs in the near infrared," Opt. Lett. 31, 1337-1339 (2006).
19. M. Fukuda, T. Mishima, N. Nakayama, and T. Masuda, "Temperature and current coefficients of lasing wavelength in tunable diode laser spectroscopy," App. Phys. B 100, 2, 377-382 (2010).
20. M. Vorontsov, G. Carhart, and J. Ricklin, "Adaptive phase-distortion correction based on parallel gradient-descent optimization," Opt. Lett. 22, 907-909 (1997).
21. R. Su, P. Zhou, X. Wang, Y. Ma, and X. Xu, "Active coherent beam combination of two high-power single-frequency nanosecond fiber amplifiers," Opt. Lett. 37, 497-499 (2012).
22. B. Dong, D. Ren, and X. Zhang, "Stochastic parallel gradient descent based adaptive optics used for high contrast imaging coronagraph," Res. Astron. Astrophys., 11, 997-1002 (2011).
23. J. Ziegler and N. Nichols "Optimum Settings for Automatic Controllers," Trans. ASME, 64, 759-768 (1942).
24. D. von der Linde, "Characterization of the noise in continuously operating mode-locked lasers," App. Phys. B, 39, 201-217 (1986).
25. S. Augst, T. Fan, and A. Sanchez, "Coherent beam combining and phase noise measurements of ytterbium fiber amplifiers," Opt. Lett. 29, 474-476 (2004).
26. Mention of commercial products is for information only; it does not imply endorsement or recommendation.